

Discovery of Highly Potent, Selective, and Brain-Penetrable Leucine-Rich Repeat Kinase 2 (LRRK2) Small Molecule Inhibitors

Anthony A. Estrada,^{*,†} Xingrong Liu,^{||} Charles Baker-Glenn,[∞] Alan Beresford,[○] Daniel J. Burdick,[†] Mark Chambers,[∞] Bryan K. Chan,[†] Huifen Chen,[†] Xiao Ding,^{||} Antonio G. DiPasquale,[●] Sara L. Dominguez,[‡] Jennafer Dotson,[†] Jason Drummond,[§] Michael Flagella,[⊥] Sean Flynn,[∞] Reina Fuji,[⊥] Andrew Gill,[×] Janet Gunzner-Toste,[†] Seth F. Harris,[#] Timothy P. Heffron,[†] Tracy Kleinheinz,[§] Donna W. Lee,[⊥] Claire E. Le Pichon,[‡] Joseph P. Lyssikatos,[†] Andrew D. Medhurst,[×] John G. Moffat,[§] Susmith Mukund,[#] Kevin Nash,[×] Kimberly Scarce-Levie,[‡] Zejuan Sheng,[‡] Daniel G. Shore,[†] Thuy Tran,[†] Naimisha Trivedi,[∞] Shumei Wang,[†] Shuo Zhang,[‡] Xiaolin Zhang,^{||} Guiling Zhao,[†] Haitao Zhu,[‡] and Zachary K. Sweeney^{†,▽}

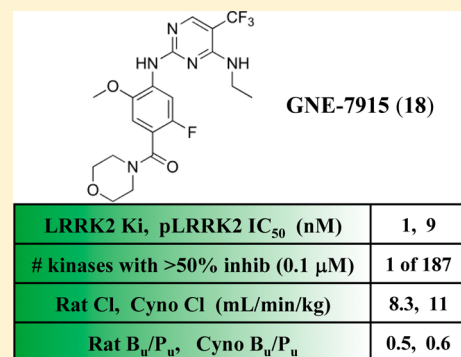
[†]Department of Discovery Chemistry, [‡]Department of Neurosciences, [§]Department of Biochemical and Cellular Pharmacology, ^{||}Department of Drug Metabolism and Pharmacokinetics, [⊥]Department of Safety Assessment, and [#]Department of Structural Biology, Genentech, Inc., 1 DNA Way, South San Francisco, California 94080, United States

[∞]Department of Chemistry, [×]Department of Biochemical and Cellular Pharmacology, and [○]Department of Drug Metabolism and Pharmacokinetics, BioFocus, Chesterford Research Park, Saffron Walden, CB10 1XL, United Kingdom

[●]X-ray Crystallographic Facility, University of California—Berkeley, 32 Lewis Hall, Berkeley, California 94720, United States

Supporting Information

ABSTRACT: There is a high demand for potent, selective, and brain-penetrant small molecule inhibitors of leucine-rich repeat kinase 2 (LRRK2) to test whether inhibition of LRRK2 kinase activity is a potentially viable treatment option for Parkinson's disease patients. Herein we disclose the use of property and structure-based drug design for the optimization of highly ligand efficient aminopyrimidine lead compounds. High throughput in vivo rodent cassette pharmacokinetic studies enabled rapid validation of in vitro–in vivo correlations. Guided by this data, optimal design parameters were established. Effective incorporation of these guidelines into our molecular design process resulted in the discovery of small molecule inhibitors such as GNE-7915 (18) and 19, which possess an ideal balance of LRRK2 cellular potency, broad kinase selectivity, metabolic stability, and brain penetration across multiple species. Advancement of GNE-7915 into rodent and higher species toxicity studies enabled risk assessment for early development.



INTRODUCTION

Parkinson's disease (PD) is the second most common neurodegenerative disease and affects approximately 1 in 100 people over the age of 60. A disease-modifying or neuroprotective therapy is highly desired, as the current standard of care is limited to symptomatic treatment.¹

In the past decade, the LRRK2 gene, which encodes a large, multidomain protein, has been linked to familial PD.^{2–6} Furthermore, the autosomal dominant G2019S kinase domain variant has been associated with both familial and idiopathic PD.^{7–9} Numerous reports have been published that suggest that the kinase activity of LRRK2 is involved in Parkinson's disease pathophysiology.^{10–17} Some of the small molecule inhibitors disclosed in these reports are highly selective for LRRK2 and could serve as useful tool compounds for examination of LRRK2 function in the periphery.^{18–20} This is critical as LRRK2 is expressed in kidney, lung, spleen,

monocytes, etc., and roles in immunology, inflammatory bowel disease, cancer, and leprosy have been proposed.^{21,22} However, the utility of these inhibitors for studying the role of LRRK2 in PD is limited, as they either do not sufficiently cross the blood–brain barrier or do not demonstrate inhibition of kinase activity in rodent brains.²³

Our group has demonstrated the in vivo inhibition of LRRK2 autophosphorylation of serine 1292 (Ser1292) in the brains of transgenic mice using a potent, selective, and brain-penetrable tool compound (7); the discovery and characterization of this autophosphorylation site are described elsewhere.^{24,26} The moderate total plasma (~150 nM) and brain (~100 nM) concentrations of 7 required to significantly inhibit LRRK2

Received: July 12, 2012

Published: September 17, 2012

kinase activity *in vivo* provide further support for LRRK2 as a potentially druggable target for PD.

We recently reported the construction of a JAK2-based LRRK2 homology model that was used to detect several binding site residues that impart general kinase selectivity.²⁵ Through a matched molecular pair activity cliff analysis we were able to identify an amino acid near the hinge binding region (Leu1949) as a selectivity hotspot.^{27–32} As illustrated in Figure 1, small ortho-substituents, such as the methoxy group in 2,4-

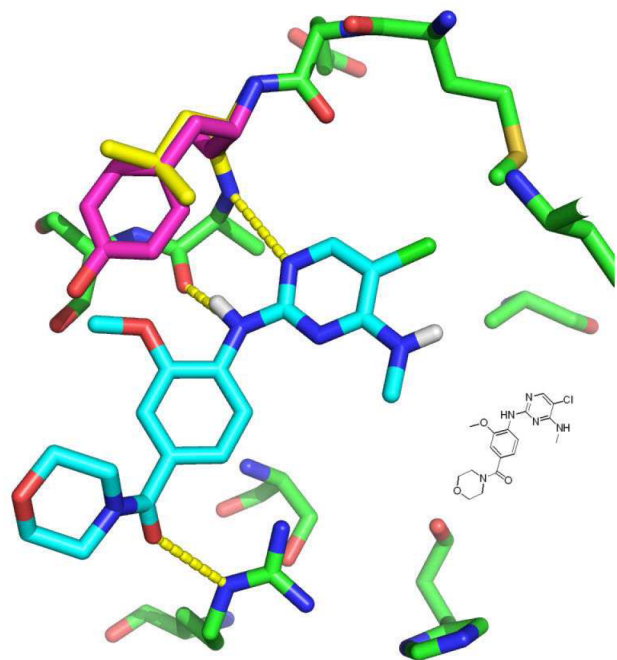


Figure 1. Docking model of **1** (cyan) in LRRK2 (green with L1949 in yellow). The side chain of Y931 of JAK2 is also shown (magenta). Intermolecular hydrogen bond interactions are shown as yellow dashed lines.

diaminopyrimidine **1**, are well tolerated in LRRK2 but are disfavored in JAK2 and approximately 290 other kinases that contain a larger Phe or Tyr residue in this binding site region near the hinge.^{25,33,34} This finding allowed us to use structure-

based drug discovery to successfully optimize a series of diaminopyrimidine inhibitors that led to the identification of **1** as a potent, selective, and brain penetrable LRRK2 small molecule inhibitor.²⁵ Compound **1**, originally disclosed in a 2011 Genentech patent application,³⁵ was subsequently used to demonstrate *in vivo* inhibition of Ser910 and Ser935 phosphorylation in mouse brain.³⁶ In this contribution we report the expanded profiling of **1** and our subsequent lead optimization efforts to identify a LRRK2 small molecule inhibitor suitable for progression to higher species toxicity studies and early development evaluation.

RESULTS AND DISCUSSION

As previously reported,²⁵ **1** has a LRRK2 biochemical potency of 3 nM (Table 1), a JAK2 biochemical selectivity index of >1067× and only inhibits wild-type and G2019S mutant LRRK2 at greater than 50% inhibition at 1 μM (345-fold over K_i) in a representative Invitrogen panel of 63 kinases. At this stage of lead optimization, the JAK2 biochemical assay proved to be a useful barometer for general kinase selectivity. In order to determine the cellular activity of **1**, we measured the inhibition of LRRK2 autophosphorylation in HEK293 cells using our LRRK2 cellular assay.²⁴ As shown in Table 1, the phospho-LRRK2 (pLRRK2) cellular IC_{50} of **1** was 29 nM, translating into an enzyme-to-cell shift of approximately 10-fold. With the cellular assay in place, we explored structure–activity relationships (SARs) of the aminopyrimidine C-4 and C-5 positions. The examples shown in Table 1 demonstrate good biochemical (<10 nM) and cellular activities (<70 nM) with the exception of aminopyrimidine C-5 fluoro (**5**) and C-5 cyano (**6**) analogues. The rationale for this observation was that C-5 groups with increased lipophilicity and size are able to interact more favorably with the gatekeeper Met1947 residue. Furthermore, all of the examples in Table 1 possess desirable CNS MPO scores³⁷ and are highly efficient as measured by lipophilic ligand efficiency (LLE)³⁸ and ligand-efficiency-dependent lipophilicity (LELP)³⁹ parameters with scores that are in line with CNS marketed drugs and clinical candidates.⁴⁰ The optimal C-4/C-5 combination proved to be the C-4 aminomethyl/C-5 trifluoromethyl substituted aminopyrimidine (i.e., **7**, pLRRK2 IC_{50} of 9 nM).

Table 1. Representative Aminopyrimidine SAR for C-4/C-5 Substitution Combinations

compd	R ¹	R ²	CNS MPO score	LRRK2 K_i^a (nM)	LLE	LELP	JAK2 selectivity Index ^b	pLRRK2: IC_{50}^c (nM)
1	Cl	NHMe	5.4	3	6.6	4.2	>1067	29
2	Cl	OMe	5.6	9	5.7	5.3	>360	69
3	Br	NHMe	5.1	2	6.8	4.3	1546	13
4	Br	OMe	5.2	5	6.0	5.4	>661	53
5	F	NHMe	5.5	58	5.8	3.6	>55	418
6	CN	NHMe	4.7	11	6.9	2.4	>288	105
7	CF ₃	NHMe	5.1	2	6.6	5.0	>1928	9

^aBiochemical assay. ^b(JAK2 K_i)/(LRRK2 K_i). ^cCellular assay.

Table 2. Rat in Vitro and in Vivo PK Profiles of Aminopyrimidines^a

compd	hepatocytes Cl_{hep}^b ($\text{mL min}^{-1} \text{kg}^{-1}$), h/r ^c	% rat PPB	Cl (Cl_p) ^d ($\text{mL min}^{-1} \text{kg}^{-1}$)	iv $t_{1/2}$ (h)	F (%)	MDR1 ^e $P_{\text{app}}^{\text{A-B}}^f$ ($\times 10^{-6} \text{cm}^2/\text{s}$)	MDR1 P-gp ER ^g (B-A ^h /A-B ^f)	B_u/P_u ⁱ	CSF/ P_u ^j
1	4.9/24.3	91.8	51 (616)	0.46	64	4.4	2.8	0.17	0.29
2	1.8/4.4	94.6	9.8 (183)	0.83	106	8.2	0.8	0.23	0.84
4	12/16	96.6	5.7 (167)	0.67	58	5.6	1.4	0.10	0.18
6	2.1/5.4	83.5	4.4 (27)	1.1	117	3.1	6.8	0.08	0.19
7	1.8/7.6	86.3	24 (156)	1.2	80	18.2	1.2	0.50	0.48

^aCompound dosed po (1 mg/kg) as a suspension in MCT and iv (0.5 mg/kg) as a 60% PEG solution or 20–60% NMP solution for systemic PK and iv as a 60% NMP solution for brain PK. ^bIn vitro stability in cryopreserved hepatocytes. ^ch/r = human/rat. ^d Cl_u = unbound clearance = total clearance/[(100 – % rat PPB)/100]. ^eMDCK-MDR1 human P-gp transfected cell line. ^fA–B, apical-to-basolateral. ^gEfflux ratio. ^hB–A, basolateral-to-apical. ⁱUnbound brain/unbound plasma AUC ratio. ^jCSF/unbound plasma AUC ratio.

The rationale for installing the aminopyrimidine C-5 trifluoromethyl group in **7** was not limited to increasing the activity for LRRK2 by providing optimal lipophilic contact with the Met gatekeeper. We also hypothesized that the trifluoromethyl group would impart a more favorable DMPK profile in comparison to other C-5 substituents because of the relative decreased oxidation potential of the pyrimidine ring system. The increased lipophilicity of the trifluoromethyl group should also favor blood–brain barrier penetration.

In order to test this hypothesis, the DMPK profiles of selected analogues from Table 1 were assessed (Table 2). Rat was employed as the primary rodent species for exploratory in vivo pharmacokinetic (PK) studies. In order to accurately assess the brain penetration of multiple compounds, we utilized a cassette dosing approach that provided brain, plasma, and CSF AUC ratios at 0.25, 1, and 3 h time points.⁴¹ Using in vitro PPB and BPB values, we then converted total brain/plasma (B/P) and total CSF/plasma (CSF/P) to unbound brain/unbound plasma (B_u/P_u) and CSF/unbound plasma (CSF/ P_u) ratios. This methodology proved to be an extremely critical resource for our program and enabled the rapid generation of meaningful in vitro MDR1 efflux ratio–in vivo unbound brain concentration correlations for medicinal chemistry design and inhibitor evaluation (vide infra).

In initial rat pharmacokinetic experiments, the previously reported aminopyrimidine lead (**1**)²⁵ was cleared rapidly from plasma and demonstrated substantial brain penetration impairment ($B_u/P_u = 0.17$, Table 2). The reduced CNS penetration was consistent with a moderate MDR1 efflux ratio (ER (B–A)/(A–B) = 2.8). While this stands in contrast to the previously reported mouse B_u/P_u ratio of 0.61, studies with P-gp/Bcrp knockout mice also suggested that **1** was an efflux substrate.²⁵ Additionally, **1** exhibited potent time-dependent inhibition (TDI) of CYP1A2. By converting the C-4 aminomethyl in **1** to a C-4 methoxy (**2**), we were able to remove one hydrogen bond donor (HBD) and achieve a 5-fold reduction in total clearance and also eliminate TDI concerns. Additionally, this modification improved the passive permeability (A–B of 4.4 to $8.2 \times 10^{-6} \text{cm}^2/\text{s}$, Table 2) and attenuated P-gp efflux (ER of 2.8 to 0.8, Table 2). Unfortunately, we quickly discovered that most C-4 methoxy analogues suffered from high brain protein binding and suboptimal B_u/P_u ratios. For inhibitor **6**, despite the extremely low Cl_u ($27 \text{mL min}^{-1} \text{kg}^{-1}$), the lack of brain exposure ($B_u/P_u = 0.08$) as predicted by in vitro MDR1 data (ER = 6.8) and poor cellular activity (105 nM, Table 1) resulted in deprioritization of C-5 cyano analogues.

Finally, as we had hypothesized (vide supra), **7** provided a desirable balance between in vivo stability, oral exposure, and brain penetration. Good CNS penetration for this compound

was achieved despite the presence of two HBDs and an amide functionality, both of which may be considered undesirable for crossing the blood–brain barrier. However, the small molecule X-ray crystal structure of **7** (Figure 2) suggests that

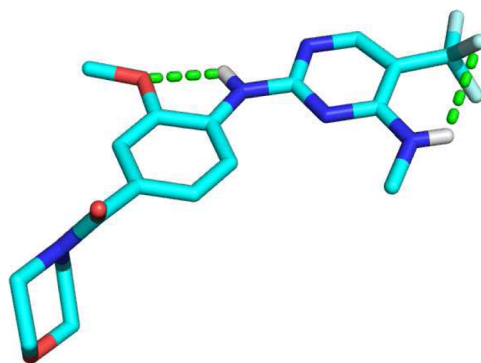


Figure 2. Small molecule X-ray crystal structure of **7** with suggested intramolecular hydrogen bonds in green.

intramolecular hydrogen bonds are formed between a fluorine of the C-5 trifluoromethyl group and the C-4 aminomethyl N–H,^{42,43} as well as the aniline N–H and the methoxy group. These interactions likely increase passive permeability and reduce the susceptibility to efflux by P-gp and/or other transporters.⁴⁴ The crystal structure also confirms the role of the amide group in reducing planarity, which is important for improving solubility and minimizing CYP inhibition.^{45,46} Inhibitor **7** is also stable in human hepatocytes ($Cl_{\text{hep}} = 1.8 \text{mL min}^{-1} \text{kg}^{-1}$) and the rat CSF levels correlate well with the measured unbound brain concentration.^{47,48} These data, along with the PK/PD analysis for **7** illustrating robust in vivo inhibition of LRRK2 autophosphorylation at Ser1292 in the brains of G2019S transgenic mice,²⁴ provided strong support for additional profiling of **7** and structurally related compounds.

Initial Invitrogen kinase selectivity profiling of **7** at 0.1 μM (178 kinases, 60-fold over LRRK2 K_i ; 0 kinases at >50% inhibition) and 1 μM (63 kinases, 600-fold over LRRK2 K_i ; 0 kinases at >80% inhibition) demonstrates that **7** is likely to be a highly selective inhibitor for LRRK2. In order to ensure that we were including all structurally related kinases in our screening panels, we re-evaluated the ATP binding site sequences of all human kinases to identify those that have either a high ATP binding site sequence identity to LRRK2 or a combination of a Met gatekeeper and a small residue such as Leu, Val, Cys, or Ala at the Leu1949 position. We found 41 kinases that met these criteria. Of the 11 of these that were available at Invitrogen and were not represented in our original panels, only

TTK (MPS1) was inhibited by several of our lead compounds. Compound 7, for example, inhibited TTK activity by 55% at 0.1 μM and 98% at 1 μM . A TTK Lanthascreen assay provided a K_i of 25 nM for 7, which translates to a biochemical TTK selectivity index of 13 \times .⁴⁹ Because of the structural homology between LRRK2 and TTK, as well as potential toxicity concerns (vide infra), it was decided that an increased TTK selectivity index was desirable.

In an attempt to introduce additional TTK selectivity while maintaining the desirable attributes of 7, we examined the inhibitor binding site residue differences between a published TTK crystal structure (magenta, PDB code 3GFW)⁵⁰ and the LRRK2 homology model (green) with 7 (cyan) docked in TTK (Figure 3). The Cys604 TTK residue is smaller than

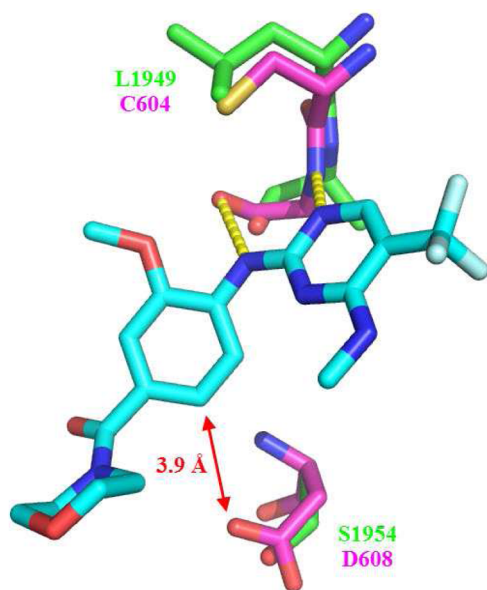


Figure 3. Key residue differences between LRRK2 homology model (green) and TTK X-ray structure (magenta) with 7 (cyan) docked in TTK. Hydrogen bond interactions between the TTK hinge residue Gly605 and 7 are shown as yellow dashed lines. The red arrow shows the measured distance between C-5' of 7 and the side chain carboxyl oxygen of Asp608.

Leu1949, supporting the lack of selectivity imparted by the *o*-methoxy group that serves as the key selectivity handle for many kinases with larger residues at this position. Additionally, both TTK and LRRK2 have Met gatekeepers. However, our analysis suggested that we may be able to exploit the Ser1954 (LRRK2) to Asp608 (TTK) residue difference by adding substituents at C-5' of the front pocket phenyl ring (para to the methoxy group) and introducing unfavorable steric and electrostatic interactions with the bulkier, negatively charged Asp608 side chain. The estimated distance from C-5' of docked 7 (cyan) to the Asp608 side chain carboxyl oxygen is approximately 3.9 Å. Thus, relatively small substituents were anticipated to clash with the Asp608 side chain and provide an increased TTK selectivity index.

In addition to the lack of TTK selectivity, we also discovered that 7 induced micronuclei formation at low concentrations in a human peripheral blood lymphocyte in vitro assay and in a mouse in vivo micronucleus study at multiple doses. While TTK has not been previously implicated in in vitro genotoxicity findings,⁵¹ the role of TTK in cell-cycle checkpoint assembly raised some concern that in vitro genotoxicity could be linked to TTK inhibition and further supported our decision to identify compounds with greater TTK selectivity.⁵² Guided by the structural insight described above, we therefore designed the phenyl C-5' substituted small molecule inhibitors shown in Table 3.

Phenyl C-5' chloro (8, Table 3) and methoxy (9, Table 3) substituted matched pairs of 7 provided clear support for the TTK selectivity hypothesis as the biochemical TTK selectivity index increased from 13 \times in 7 to 53 \times and 275 \times , respectively. These compounds also maintained desirable LRRK2 cellular activities (7 and 21 nM). Desirable selectivity indices over JAK2 and TTK were also achievable with chlorine as the C-2' JAK selectivity handle and methoxy at C-5' (10 and 11). Expanded kinase profiling (189 kinases) at 1 μM demonstrated excellent selectivity for both 10 (250-fold over LRRK2 K_i ; 0 kinases at >75% inhibition) and 11 (345-fold over LRRK2 K_i ; only two kinases at >80% inhibition). Thus, TTK and JAK2 biochemical assays were incorporated into our screening cascade as off-target counterscreens and served as robust indicators of general kinase selectivity for new compounds.

After the TTK selectivity issues were addressed, the in vitro and in vivo DMPK profiles of phenyl 2',5' substituted analogues 8–12 were assessed (Table 4). The plasma protein

Table 3. Preliminary Investigation of Phenyl 2',5'-Substitution for Increased TTK Selectivity

compd	R ¹	R ²	R ³	LRRK2 K_i ^a (nM)	JAK2 selectivity index ^b	TTK selectivity index ^c	pLRRK2 IC ₅₀ ^d (nM)
7	Me	OMe	H	2	>1928	13	9
8	Me	OMe	Cl	2	>1368	53	7
9	Me	OMe	OMe	1	>2540	275	21
10	Me	Cl	OMe	4	>808	105	24
11	Et	Cl	OMe	3	>1096	77	27

^aBiochemical assay. ^b(JAK2 K_i)/(LRRK2 K_i). ^c(TTK K_i)/(LRRK2 K_i). ^dCellular assay.

Table 4. Rat in Vitro and in Vivo PK Profiles of Phenyl 2',5'-Substituted Aminopyrimidines 8–12^a

compd	hepatocytes Cl_{hep}^b ($mL\ min^{-1}\ kg^{-1}$), h/r ^c	% rat PPB	Cl (Cl_p) ^d ($mL\ min^{-1}\ kg^{-1}$)	iv $t_{1/2}$ (h)	F (%)	MDR1 ^e P_{app}^f A–B ^f ($\times 10^{-6}\ cm/s$)	MDR1 P-gp ER ^g (B–A ^h /A–B ^f)	B_u/P_u ⁱ	CSF/ P_u ^j
8	2.8/22	99.1	4.7 (551)	1.1		8.1	1.9	0.11	0.41
9	0.8/15.2	91.4	15 ^k (170)	1.2	101	4.4	3.4	0.80	2.0
10	0.8/3.7	90.8	59 ^k (640)	0.83	48	10.4	1.1	0.72	1.8
11	0.9/26	96.3	19 ^k (514)	1.2	47	8.3	1.6	0.77	2.9
12 ^l	5.7/14	95.5	10 ^k (227)	2.5	66	8.5	1.3		

^aCompound dosed po (1 mg/kg) as a suspension in MCT and iv (0.5 mg/kg) as a 60% PEG solution or 20–60% NMP solution for systemic PK and iv as a 60% NMP solution for brain PK. ^bIn vitro stability in cryopreserved hepatocytes. ^ch/r = human/rat. ^d Cl_u = unbound clearance = total clearance/[(100 – % rat PPB)/100]. ^eMDCK-MDR1 human P-gp transfected cell line. ^fA–B, apical-to-basolateral. ^gEfflux ratio. ^hB–A, basolateral-to-apical. ⁱUnbound brain/unbound plasma AUC ratio. ^jCSF/unbound plasma AUC ratio. ^kBlood clearance is reported. ^lMorpholine-*d*₈ analogue of 11.

binding of 8 was unexpectedly high, resulting in an unbound clearance ($551\ mL\ min^{-1}\ kg^{-1}$) 3.5-fold higher than 7 and an unacceptable B_u/P_u ratio of 0.11. Despite showing slight MDR1 efflux with the human P-gp cell line, dimethoxy analogue 9 demonstrated an in vivo profile comparable to that of 7. While 9 did not reveal any covalent adducts from in vitro trapping studies with glutathione, we ultimately decided not to pursue this compound because of concerns regarding electrophilic metabolites that might be formed from oxidation of the electron-rich phenyl ring. The excellent brain penetration of 10 was promising ($B_u/P_u = 0.77$); however, a large in vitro–in vivo (iviv) disconnect resulted in a clearance higher than liver blood flow. As a result of significant N-demethylation observed from in vitro metabolite identification studies, the aminoethyl analogue of 10 (11) was prepared and successfully reduced the total clearance while maintaining comparable brain penetration. Both 10 and 11 also demonstrated significant in vitro oxidative metabolism of the morpholine ring. Thus, in an attempt to further reduce the metabolic turnover, the morpholine-*d*₈ analogue (12) of 11 was synthesized and reduced the clearance significantly, presumably because of kinetic deuterium isotope effects.⁵³

As previously mentioned, 7 demonstrated genotoxicity at low concentrations. This is a concern for an indication that potentially requires chronic dosing from an early age. Therefore, 10 and 11 were chosen for in vitro analyses in a human peripheral blood lymphocyte genotoxicity assay. While we were pleased to find that both parent molecules did not induce micronuclei formation, incubation of 11 with S9 fraction revealed the formation of potentially clastogenic metabolites. Since the in vitro metabolite profile of deuterated morpholine analogue 12 was similar to that of 11, these molecules were deprioritized.

At this point in our program, we had established reliable metabolic stability and permeability iviv correlations with a wide range of aminopyrimidines, including those already illustrated. These relationships were used to rapidly triage newly synthesized molecules prior to in vivo evaluation, and their associated physicochemical property ranges provided useful guidelines at the design stage. For example, retrospective analysis revealed that analogues with a cLogD between 1.8 and 3.3 had the highest probability (60%) of being metabolically stable in human hepatocytes (Figure 4A). While inhibitors with a cLogD < 1.8 also demonstrated good stability, most of these compounds were P-gp efflux substrates. Most analogues with TPSA < 90 showed a low propensity for P-gp efflux (85% exhibited an efflux ratio of <3, Figure 4B). Thus, the application of refined design parameters (1.8 < cLogD < 3.3 and TPSA < 90)⁵⁴ for future analogues in this series was adopted to increase

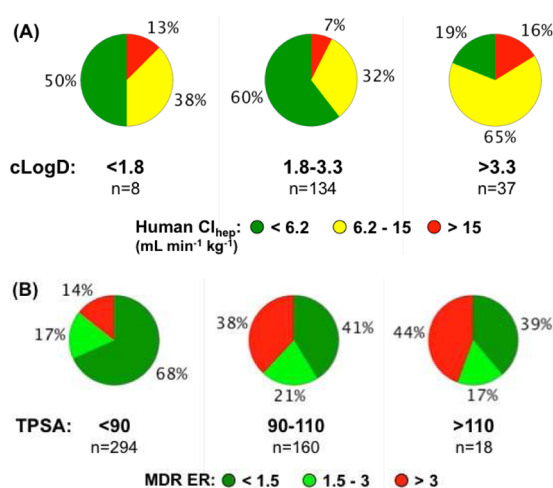
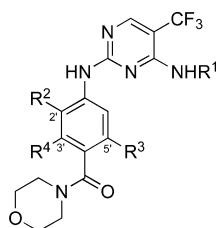


Figure 4. Vortex charts illustrating (A) binned cLogD (pH 7.4) values for aminopyrimidines colored by in vitro human hepatocyte stability measured from cryopreserved hepatocytes and (B) binned TPSA values for aminopyrimidines colored by MDCK-MDR1 efflux ratios (ER), Vortex, version 2012.02.13219.

our probability of success and ultimately reduce the number of compounds synthesized prior to nomination for development.

With several molecules already demonstrating fairly optimized activity, selectivity, and ADME profiles within the aminopyrimidine scaffold, our goal was to make subtle improvements while staying within the desirable property ranges. This focus led to the alternative phenyl substitution patterns shown in Table 5. C-5' methyl analogues 13 and 14 displayed good TTK selectivity, with the latter also possessing good LRRK2 cellular activity. In an attempt to maintain acceptable selectivity indices while reducing both molecular weight and lipophilicity, various methoxy/fluoro combinations were targeted (15–19, Table 5). 15 demonstrated excellent kinase selectivity when tested against 189 kinases at 1 μM (135-fold over LRRK2 K_i ; 0 kinases at >75% inhibition); however, the LRRK2 cellular activity for 15 (63 nM) was suboptimal. Inhibitor 16, which lacked a C-5' group, was even less selective for TTK than 7 and confirmed the necessity for a substituent at C-5'. Simply shifting the fluorine from C-3' to C-5' (17) restored the biochemical TTK selectivity index to greater than 50 \times while also increasing affinity for LRRK2. Maintaining the methoxy/fluoro arrangement at C-2'/C-5' and varying aminoalkyl R^1 substitution resulted in single-digit nanomolar LRRK2 cellular activities for GNE-7915 (18, 9 nM, R^1 = aminoethyl) and 19 (4 nM, R^1 = aminocyclopropyl). Expanded Invitrogen kinase profiling (187 kinases) at 0.1 μM for both 18 (100-fold

Table 5. Aminopyrimidine Phenyl 2',3',5'-Substitution SAR



compd	R ¹	R ²	R ³	R ⁴	LRRK2 K _i ^a (nM)	JAK2 selectivity index ^b	TTK selectivity index ^c	pLRRK2 IC ₅₀ ^d (nM)
13	Me	Cl	Me	H	7	>489	78	43
14	Me	OMe	Me	H	2	>1871	387	11
15	Me	F	OMe	H	7	189	106	63
16	Me	OMe	H	F	12	>262	11	35
17	Me	OMe	F	H	6	>533	62	16
18	Et	OMe	F	H	1	>3200	53	9
19	cPr	OMe	F	H	1	>3200	118	4

^aBiochemical assay. ^b(JAK2 K_i)/(LRRK2 K_i). ^c(TTK K_i)/(LRRK2 K_i). ^dCellular assay.

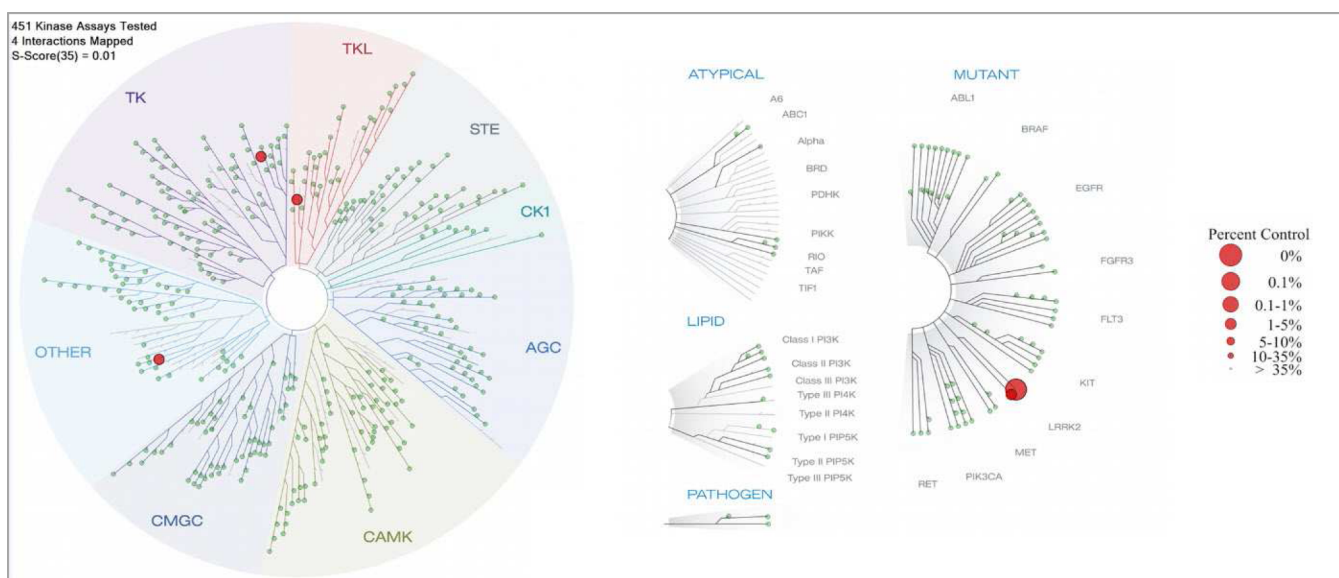


Figure 5. KinomeScan selectivity tree for **18** at 0.1 μ M (100-fold over LRRK2 K_i). Of 451 profiled kinases, only LRRK2, TTK, and ALK demonstrated <35% inhibition of % control (>65% probe displacement).

Table 6. Rat in Vitro and in Vivo PK Profiles of Phenyl 2',5'-Substituted Aminopyrimidines **14** and **17**–**19**^a

compd	hepatocytes (mL min ⁻¹ kg ⁻¹), h/r ^c	Cl _{hep} ^b (h/r ^c)	% rat PPB	Cl (Cl _p) ^d (mL min ⁻¹ kg ⁻¹)	iv t _{1/2} (h)	F (%)	MDR1 ^e P _{app} , A–B ^f (×10 ⁻⁶ cm/s)	MDR1 P-gp ER ^g (B–A ^h /A–B ^f)	B _u /P _u ⁱ	CSF/P _u ^j
14	4.2/22		95.8	28 (667)	1.2	46	5.0	3.1	0.88	2.1
17	3.9/11		95.7	12 (279)	4.2	79	3.3	2.2	0.15	0.28
18	3.2/14		96.6	8.3 (244)	3.1	40	10.4	0.9	0.50	0.60
19	4.9/15		97.6	6.8 (296)	6.0	65	10.9	1.3	0.61	0.27

^aCompound dosed po (1 mg/kg) as a suspension in MCT and iv (0.5 mg/kg) as a 60% PEG solution or 20–60% NMP solution for systemic PK and iv as a 60% NMP solution for brain PK. ^bIn vitro stability in cryopreserved hepatocytes. ^ch/r = human/rat. ^dCl_p = unbound clearance = total clearance/[(100 – % rat PPB)/100]. ^eMDCK-MDR1 human P-gp transfected cell line. ^fA–B, apical-to-basolateral. ^gEfflux ratio. ^hB–A, basolateral-to-apical. ⁱUnbound brain/unbound plasma AUC ratio. ^jCSF/unbound plasma AUC ratio.

over LRRK2 K_i) and **19** (250-fold over LRRK2 K_i) resulted in only TTK showing greater than 50% inhibition. Selectivity profiling using the DiscoverX KinomeScan⁵⁵ competitive binding assay panel, which included 392 unique kinases, was also performed for **18** at 0.1 μ M (Figure 5). Binding of >50% probe displacement was detected for 10 kinases and of >65% for only LRRK2, TTK, and ALK, further supporting the

excellent LRRK2 selectivity for **18**. Cerep receptor profiling, including expanded brain panels, suggested that **18** and **19** only inhibited 5-HT_{2B} with >70% inhibition at 10 μ M. **18** and **19** were confirmed to be moderately potent 5-HT_{2B} antagonists in in vitro functional assays.⁵⁶

The DMPK profiles of the most promising compounds from Table 5 were then assessed (Table 6). Inhibitor **14** was

Table 7. SAR and DMPK Profiles of Aminopyrimidines 20–25^a

compd	R ¹	R ²	LRRK2 K _i ^b (nM)	TTK Selectivity Index ^c	pLRRK2 IC ₅₀ ^d (nM)	Cl (Cl _u) ^e (mL min ⁻¹ kg ⁻¹)	F (%)	MDR1 ^f P-gp ER ^g (B-A/A-B) ^h	B _u /P _u ⁱ
20	Me		8	3.3	100	16 (328)	24	0.7	0.65
21	Me		2	27	27	20 (325)	27	1.3	0.70
22	Et		3	63	17	7.9 (31)	50	2.0	0.08
23	Me		9	11	51	38 ^j (304)	39	0.7	0.61
24	Et		1	43	10	4.3 (195)	52	0.9	0.26
25	Et		4	6.4	22	11 (228)	93	1.6	0.11

^aCompound dosed po (1 mg/kg) as a suspension in MCT and iv (0.5 mg/kg) as a 60% PEG solution or 20–60% NMP solution for systemic PK and iv as a 60% NMP solution for brain PK. ^bBiochemical assay. ^c(TTK K_i)/(LRRK2 K_i). ^dCellular assay. ^eCl_u = unbound clearance = total clearance/[(100 – % rat PPB)/100]. ^fMDCK-MDR1 human P-gp transfected cell line. ^gefflux ratio. ^hA:B, apical-to-basolateral; B:A, basolateral-to-apical. ⁱUnbound brain/unbound plasma AUC ratio. ^jBlood clearance is reported.

moderately cleared as predicted by in vitro measurements and demonstrated good metabolic stability in human hepatocytes. It also displayed good in vivo brain penetration. Compound 17 also showed a strong iviv correlation with respect to metabolic clearance; however, the B_u/P_u ratio of 0.15 was suboptimal. Both 18 and 19 demonstrated excellent in vitro DMPK and in vivo rat PK profiles: (a) minimal turnover in human hepatocytes; (b) low total and unbound clearance values as predicted by rat hepatocytes; (c) long half-lives and good oral exposure; (d) high passive permeability, no human P-gp efflux, and good brain penetration in rats. Having established the lead profiles of 14, 18, and 19 as benchmarks, additional SAR exploration was carried out to address specific areas that we felt could potentially be improved upon.

As amides are often substrates for P-gp, one approach to improve brain penetration of our current leads was to introduce amide isosteres such as tetrazole 20 (Table 7). Indeed, 20 did exhibit good brain exposure (B_u/P_u = 0.65); however, poor solubility, relatively modest LRRK2 cellular activity, and mild CYP1A2 TDI precluded further advancement. Similar tetrazoles, triazoles, pyrazoles, and other heterocyclic replacements showed promising brain exposure, but most suffered from a combination of poor solubility and time-dependent inhibition of CYP1A2. Alkylsulfones were also investigated as amide replacements. Representative of this series, 21 showed good in vivo stability and brain PK (B_u/P_u = 0.70); however, the alkylsulfones were compromised by time-dependent inhibition of CYP1A2, poor solubility, and interestingly, inadequate kinase selectivity. These observations are consistent with the notion that the morpholinoamide functionality of the primary series of inhibitors is optimal for decreasing inhibitor planarity and improving solubility.^{57,58} Pyridine replacement of the phenyl ring was also conducted to improve solubility and gauge whether or not the C-5' nitrogen lone pair could serve as a suitable TTK selectivity handle. 22 provided support for this

hypothesis, as it showed a 63-fold selectivity TTK index. Unfortunately, although 22 exhibited optimal cellular activity, unbound clearance, and bioavailability, poor brain penetration prevented further profiling. Scission of the amide bond in 22 and removal of the morpholine nitrogen to avoid bis-aniline formation afforded 23. Unfortunately, while 23 and various other saturated heterocycles enhanced brain penetration, inadequate levels of TTK selectivity were obtained. Finally, several morpholine derivatives were targeted, as the morpholine ring had been identified as a major site of metabolism and an altered metabolic profile for unpredictable toxicity/genotoxicity could prove desirable. This strategy is exemplified by 24 and 25 where the intent was to minimize P-gp recognition of the introduced polarity through steric congestion (tertiary alcohols) and intramolecular hydrogen bonding (secondary amide N-H and arylfluorine). Good LRRK2 activity and in vivo metabolic clearance was achieved, but a combination of poor solubility and insufficient unbound brain levels again precluded further progression.

Lead compounds 14, 18, and 19 were further evaluated in PK/PD studies. Thus, BAC transgenic mice expressing human LRRK2 protein with the G2019S Parkinson's disease mutation were given either a single oral dose (po) or intraperitoneal (ip) injection. Brain (hippocampus) and peripheral (spleen) tissues were harvested 1–24 h postdose to assess pSer1292 levels and compound concentration.²⁴ Figure 6A shows robust, concentration-dependent knockdown of pLRRK2 in the brain after oral dosing with 18 at both 15 and 50 mg/kg and after ip dosing at both 10 and 50 mg/kg (see Supporting Information for spleen PK/PD graphs of 18, 19, and 14). By use of a pharmacodynamic inhibition model to fit the data, 18 had a calculated in vivo unbound brain IC₅₀ of 7 nM, which is consistent with the cellular IC₅₀ of 9 nM.⁵⁹ Taken together with the recently published PK/PD data for 7,²⁴ we adopted a screening PK/PD protocol that involved ip dosing at both 10

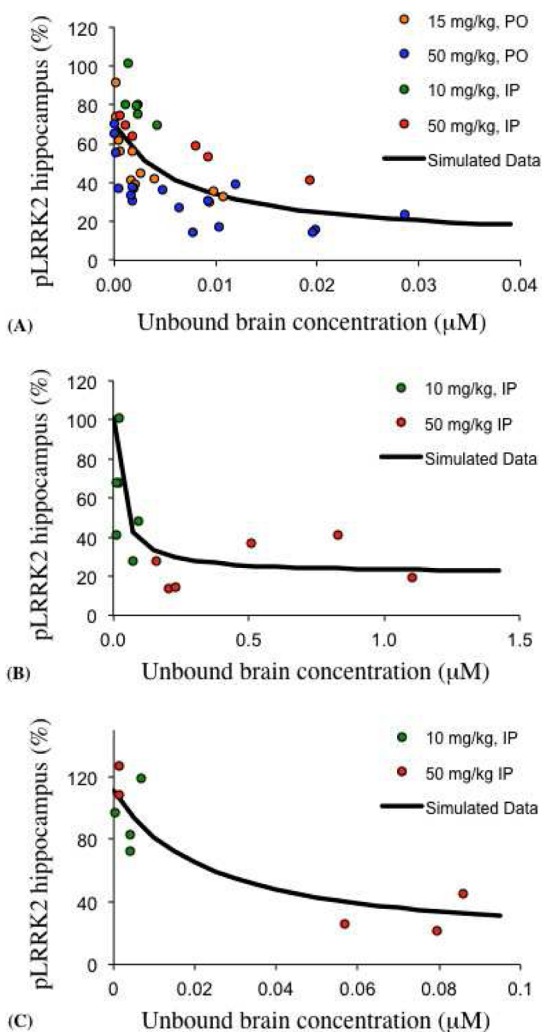


Figure 6. In vivo G2019S LRRK2 transgenic mouse PK/PD results measuring brain pSer1292 autophosphorylation. The closed circles represent the observed data, and the lines represent the predicted data from a direct inhibition model. Percent inhibition is normalized to pSer1292 levels observed in mice dosed with vehicle alone ($n = 3$). Plotted data are shown for mice treated with (A) **18** [15 mg/kg, po, at 1, 3, and 6 h ($n = 4$ /dose); 50 mg/kg, po, at 1, 3, 6, and 12 h ($n = 4$ /dose) and 24 h ($n = 1$); 10 mg/kg, ip, at 1 and 2.5 h ($n = 3$ /dose); 50 mg/kg, ip, at 1 and 6 h ($n = 3$ /dose)]; (B) **19** [10 and 50 mg/kg, ip, at 1 and 6 h ($n = 3$ /dose)]; (C) **14** [10 and 50 mg/kg, ip, at 1 and 6 h ($n = 3$ /dose)].

and 50 mg/kg with tissue collection at 1 and 6 h postdose to assess future compounds with promising profiles. In these studies, **19** and **14** also demonstrated on-target reduction of brain pLRRK2 (Figure 6B and Figure 6C) with calculated in vivo unbound brain IC_{50} of 27 nM for **19** and 24 nM for **14**.

As a result of their encouraging in vitro and in vivo profiles, **18** and **19** were both progressed to cynomolgus monkey PK

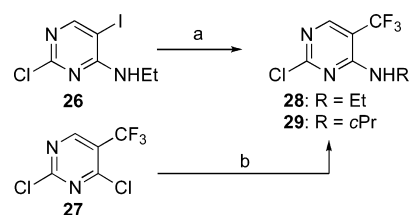
studies. As depicted in Table 8, both compounds exhibited low total and unbound plasma clearance values and long half-lives. The bioavailability for **18** at 1 mpk (17%) and 20 mpk (24%) was slightly lower than expected, especially when one considers the minimal contribution from first pass hepatic extraction. It is known, however, that compounds predominantly metabolized by CYP enzymes can demonstrate higher levels of first-pass intestinal metabolism in cynomolgus monkeys than in humans.⁶⁰ The decline in oral exposure from 1 to 20 mpk with **19** is suggestive of solubility-limited absorption.⁶¹

As the advancement of previous leads had been halted because of genotoxicity concerns, **18** was chosen for evaluation of in vivo genotoxic liabilities. Sprague–Dawley rats were administered **18** daily for 2 days at 100 mg/kg via oral gavage and assessed for the presence of micronucleated polychromatic erythrocytes in their bone marrow. Inhibitor **18** did not induce micronucleus formation, even with an approximate unbound $AUC_{(0-24h)}$ plasma concentration of 5.95 $\mu\text{M}\cdot\text{h}$. **18** was then progressed to 7-day repeat-dose toxicity studies in rats (10, 50, and 100 mg/kg) and cynomolgus monkeys (10, 25, and 65 mg/kg). The compound was well tolerated in rats after oral administration with day 7 mean unbound plasma $AUC_{(0-24h)}$ concentrations of 0.8, 3.9, and 4.7 $\mu\text{M}\cdot\text{h}$, respectively. High drug exposures were also achieved in cynomolgus monkeys with day 7 mean unbound plasma $AUC_{(0-24h)}$ concentrations of 0.8, 3.1, and 7.8 $\mu\text{M}\cdot\text{h}$, respectively. Additionally, cyno terminal brain and CSF levels measured 24 h after receiving the last dose on day 7 confirmed good brain penetration ($B_u/P_u = 0.6$ and $CSF/P_u = 0.82$). Taken together, these results indicate that **18** can be used to preclinically assess the consequences of inhibiting LRRK2 kinase activity in the brain. Full disclosure of toxicity studies performed with **18** and other aminopyrimidines will be disclosed in due course.

CHEMISTRY

The syntheses of aminoethyl (**28**) and aminocyclopropyl (**29**) 2,4-diaminopyrimidine rings are shown in Scheme 1. Scheme 2

Scheme 1. Synthesis of 2,4-Diaminopyrimidine Cores^a



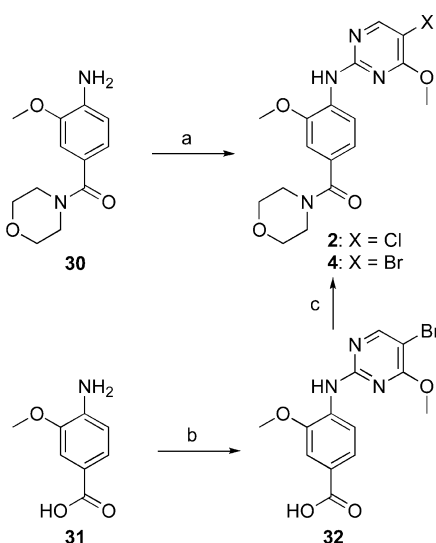
^aReagents and conditions: (a) CuI, KF, TMSCF₃, DMF, Δ , 69%; (b) *c*-PrNH₂, THF, 34%.

describes the two-step syntheses of **2** and **4** from known (**30**)²⁵ or commercially available (**31**) starting materials. Tetrasubstituted precursors for **13** and **14** are derived from anilines **33** and **34** (Scheme 3) via a Sandmeyer reaction to provide

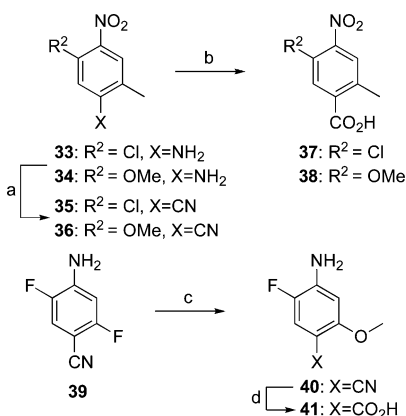
Table 8. In Vivo Cyno PK Profiles of **18** and **19**^a

compd	hepatocytes Cl_{hep} ^b (mL min ⁻¹ kg ⁻¹), cyno	% cyno PPB	Cl (Cl_u) ^c (mL min ⁻¹ kg ⁻¹)	iv $t_{1/2}$ (h)	F (%), 1 mg/kg	F (%), 20 mg/kg
18	14	94.5	11 (200)	7.7	17	24
19	9.2	95.5	3.8 (84)	10.7	105	22

^aCompound dosed po (1 and 20 mg/kg) with crystalline material as a suspension in MCT and iv (0.5 mg/kg) as a 20–60% NMP solution. ^bIn vitro stability in cryopreserved hepatocytes. ^c Cl_u = unbound clearance = total clearance/[$(100 - \% \text{ cyno PPB})/100$].

Scheme 2. Synthesis of Aminopyrimidine-4-methoxy Analogues 2 and 4^a

^aReagents and conditions: (a) 2,5-dichloro-4-methoxypyrimidine, Cs₂CO₃, Xantphos, Pd₂(dba)₃, dioxane, microwave, 15%; (b) 5-bromo-2-chloro-4-methoxypyrimidine, TFA, *n*-BuOH, microwave, 35%; (c) morpholine, HBTU, DIPEA, DMF, 56%.

Scheme 3. Synthesis of Tetrasubstituted Phenyl Intermediates for the Synthesis of 13, 14, and 15^a

^aReagents and conditions: (a) acetone, conc HCl, H₂O, NaNO₂, then CuCN, NaCN; (b) AcOH, conc H₂SO₄, H₂O, Δ; (c) *t*-BuOK, MeOH, THF, 80%; (d) KOH, EtOH, H₂O, 68%.

arylnitriles **35** and **36** followed by hydrolysis to afford carboxylic acids **37** and **38**. The precursor for **15** is generated from regioselective methoxide displacement of **39** to provide **40** (Scheme 3), followed by hydrolysis to yield benzoic acid **41**. Scheme 4 illustrates the representative syntheses of aminopyrimidine tetra- and pentasubstituted morpholinoamides. Standard amide formation from the associated benzoic acid (**41–43**) followed by acid catalyzed S_NAr or Buchwald–Hartwig coupling between anilines **44–46** and a 4-aminoalkyl-2-chloro-5-trifluoromethylpyrimidine derivative furnished an array of products. The second method used to synthesize various aminopyrimidine targets commences from morpholine amide formation of the respective *p*-nitrobenzoic acids (**37, 38, 47–49**) followed by nitro reduction and S_NAr coupling between anilines **55–59** and **60**. The third protocol used to

provide **12, 18, and 19** involved a TFA catalyzed S_NAr of anilines **42** and **43** and then peptide coupling as the final step.

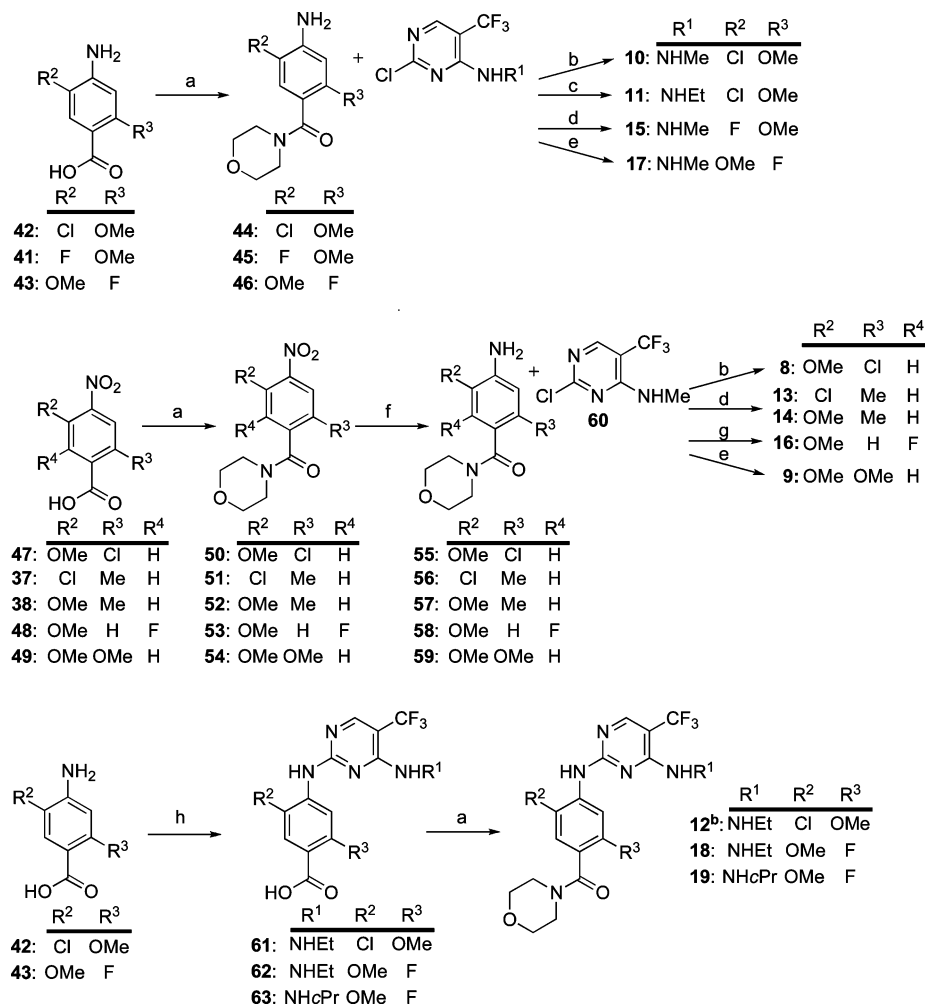
The synthesis of aminopyrimidine amide isosteres **20** and **21** is depicted in Scheme 5. **20** is derived from Buchwald–Hartwig coupling of 4-amino-3-chlorobenzonitrile **64** and 4-amino-methyl-2-chloro-5-trifluoromethylpyrimidine (**60**), followed by tetrazole formation (**66**) and methylation. Nucleophilic arylfluorine displacement with sodium thiomethoxide, *m*-CPBA oxidation to the corresponding sulfone **69**, nitro reduction, and acid catalyzed coupling of the resulting aniline **70** with 4-aminomethyl-2-chloro-5-trifluoromethylpyrimidine (**60**) yielded **21**. Scheme 6 illustrates the independent syntheses of pyridine analogues **22** and **23** as well as morpholine amide derivatives **24** and **25**. Hence, palladium catalyzed aminocarbonylation of 6-chloro-4-methoxypyridin-3-amine **71** with morpholine and Mo(CO)₆ followed by Buchwald coupling afforded **22**. The synthesis of **23** commenced with palladium catalyzed cross-coupling of 2-chloro-4-methoxy-5-nitropyridine (**73**) followed by concomitant dihydropyran and nitro reduction to give **75**. Buchwald coupling then provided the final target (**23**). Amide derivative **24** was synthesized in the same manner as **18** (Scheme 4), using 1-amino-2-methylpropan-2-ol instead of morpholine. Lastly, bromination of toluene derivative **76**, amide formation, and subsequent intramolecular lactam formation to give **78** followed by nitro reduction and standard S_NAr coupling afforded isoindolone **25**.

CONCLUSION

Starting from highly ligand efficient leads **1** and **7**, the successful development of small molecule LRRK2 inhibitors suitable for higher species toxicity studies and early development evaluation is described. Optimization of LRRK2 cellular activity through appropriate C-4/C-5 aminopyrimidine substitution was achieved while imparting broad kinase selectivity, including structurally related kinases such as TTK, through strategic decoration of the phenyl ring. We were also able to effectively balance physicochemical properties, which enabled the generation of inhibitors with excellent *in vitro* and *in vivo* DMPK profiles including minimal turnover in human hepatocytes and low unbound clearance and good oral exposure in rodents and cynomolgus monkeys. Of equal importance was the demonstrated ability of multiple compounds to penetrate the blood–brain barrier while maintaining such a well-balanced profile. Taken together, these efforts culminated in the discovery of GNE-7915 (**18**) and **19**, highly potent, selective, metabolically stable and brain-penetrant LRRK2 inhibitors with potent *in vivo* unbound brain IC₅₀ values measured from G2019S transgenic mice PK/PD studies. GNE-7915 achieved high exposures in the periphery and brain throughout a 7-day dosing regimen in both rat and cynomolgus monkey toxicity studies. A detailed report of toxicity studies and associated histopathology findings with GNE-7915 and other aminopyrimidine LRRK2 inhibitors will be disclosed in a subsequent publication.

EXPERIMENTAL SECTION

All chemicals were purchased from commercial suppliers and used as received. Flash chromatography was carried out with prepacked SiO₂ cartridges from either ISCO or SiliCycle on an ISCO Companion chromatography system using gradient elution or with prepacked silica gel cartridges from Biotage using a Biotage SP4 or an Isolera 4 MPLC system using gradient elution. NMR spectra were recorded on Bruker

Scheme 4. Synthesis of Aminopyrimidine Phenyl Tetra- and Pentasubstituted Morpholinoamides^a

^aReagents and conditions: (a) morpholine, HATU or HBTU, DIPEA, CH₂Cl₂; (b) TFA, *n*-BuOH, Δ; (c) Cs₂CO₃, Xantphos, Pd(OAc)₂, dioxane, microwave; (d) PTSA, dioxane, Δ; (e) TFA, *n*-BuOH, microwave; (f) Pd/C, MeOH, H₂ or SnCl₂·2H₂O, EtOH, H₂O, Δ or Fe dust, EtOH, NH₄Cl, H₂O, Δ; (g) *n*-BuOH, microwave; (h) 2-chloro-*N*-alkyl-5-(trifluoromethyl)pyrimidin-4-amine, PTSA, dioxane, Δ. ^bMorpholine-*d*₈ analogue.

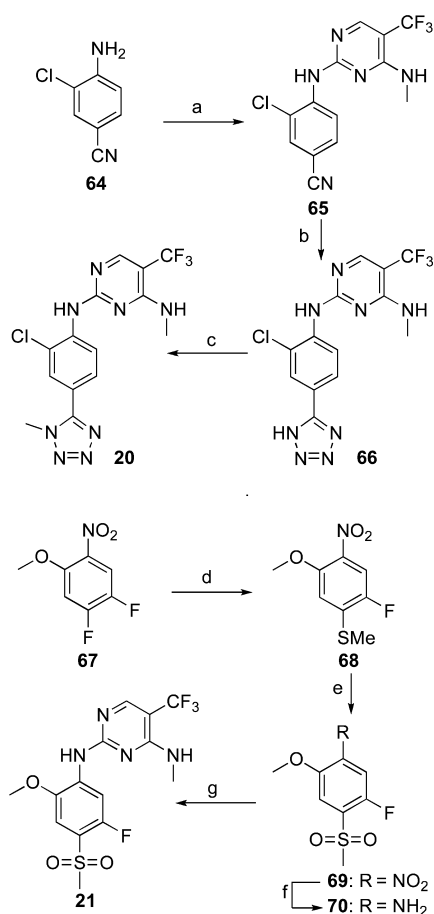
Avance 400, Bruker DPX 400M, Bruker Avance III 400, and Bruker AV III 400 or 500 NMR spectrometers and referenced to tetramethylsilane. The following abbreviations are used: br = broad signal, s = singlet, d = doublet, dd = doublet of doublets, t = triplet, q = quartet, m = multiplet. Preparative HPLC was performed on a Polaris C₁₈ 5 μm column (50 mm × 21 mm), a Waters Sunfire OBD Phenomenex Luna phenylhexyl column (150 mm × 19 mm), or a Waters Xbridge phenyl column (150 mm × 19 mm), eluting with mixtures of water–acetonitrile or water–methanol, optionally containing a modifier (0.1% v/v formic acid or 10 mM ammonium bicarbonate). Low-resolution mass spectra were recorded on a Sciex 15 mass spectrometer in ES+ mode, a Micromass ZQ single quadrupole LCMS in ES+, ES− mode, or a Quattro Micro LC–MS–MS in ES+, ES− mode. All final compounds were purified to >95% chemical and optical purity, as assayed by (a) HPLC (Waters Acquity UPLC column, 21 mm × 50 mm, 1.7 μm) with gradient of 0–90% acetonitrile (containing 0.038% TFA) in 0.1% aqueous TFA, with UV detection at λ = 254 and 210 as well as CAD detection with an ESA Corona detector or (b) HPLC (Phenomenex Luna C18 (2) column, 4.6 mm × 100 mm, 5 μm) with gradient of 5–95% acetonitrile in water (with 0.1% formic acid in each mobile phase), with UV DAD detection between λ = 210 and 400 nm; (c) HPLC (Waters Xterra MS C18 column, 4.6 mm × 100 mm, 5 μm) with gradient of 5–95% acetonitrile in water (with 10 mM ammonium bicarbonate in the aqueous mobile phase), with UV DAD detection

between λ = 210 and 400 nm; (d) HPLC (Supelco, Ascentis Express C18 or Hichrom Halo C18 column, 4.6 mm × 150 mm, 2.7 μm) with gradient of 4–100% acetonitrile in water (with 0.1% formic acid in each mobile phase), with UV DAD detection between λ = 210 and 400 nm; (e) HPLC (Phenomenex, Gemini NX C18 column, 4.6 mm × 150 mm, 3 μm) with gradient of 4.5–100% acetonitrile in water (with 10 mM ammonium bicarbonate in the aqueous mobile phase), with UV DAD detection between λ = 210 and 400 nm.

The syntheses of compounds 1, 3, 5, 6, and 7 have been described previously.²⁵

(4-(5-Chloro-4-methoxypyrimidin-2-ylamino)-3-methoxyphenyl)(morpholino)methanone (2). To a solution of (4-amino-3-methoxyphenyl)(morpholino)methanone (30, 0.490 g, 2.1 mmol) in 1,4-dioxane (7 mL) were added 2,5-dichloro-4-methoxypyrimidine (0.370 g, 2.1 mmol), Cs₂CO₃ (1.4 g, 4.1 mmol), Xantphos (0.100 g, 0.21 mmol), and Pd₂(dba)₃ (0.095 g, 0.10 mmol), and the reaction mixture was stirred at 140 °C for 25 min under microwave irradiation. The reaction mixture was filtered, concentrated, purified by flash chromatography, 0–100% EtOAc/heptane, and further purified by preparative HPLC to afford the title compound (117 mg, 15% yield). ¹H NMR (400 MHz, DMSO-*d*₆) δ 8.31 (m, 2H), 8.16 (d, *J* = 8.2 Hz, 1H), 7.08 (d, *J* = 1.3 Hz, 1H), 7.01 (dd, *J* = 8.2, 1.3 Hz, 1H), 4.00 (s, 3H), 3.89 (s, 3H), 3.61 (br s, 4H), 3.52 (br s, 4H). LCMS, *m/z* = 379 [M + H]⁺.

(4-(5-Bromo-4-methoxypyrimidin-2-ylamino)-3-methoxyphenyl)(morpholino)methanone (4). To a solution of 4-

Scheme 5. Synthesis of Aminopyrimidineamide Isosteres 20 and 21^a

^aReagents and conditions: (a) **60**, Cs₂CO₃, Xantphos, Pd₂(dba)₃, dioxane, Δ, 45%; (b) NaN₃, NH₄Cl, DMF, Δ, 85%; (c) MeI, K₂CO₃, acetone, Δ, 70%; (d) MeSNa, EtOH, Δ, 91%; (e) *m*-CPBA, CH₂Cl₂, 48%; (f) Pd/C, EtOH, H₂, 99%; (g) **60**, TFA, 2-methoxyethanol, Δ, 19%.

amino-3-methoxybenzoic acid (**31**, 1.77 g, 10.6 mmol) in *n*-BuOH (62 mL) was added 5-bromo-2-chloro-4-methoxypyridine (2.25 g, 10.1 mmol) and TFA (0.194 mL, 2.52 mmol), and the reaction mixture was stirred at 125 °C for 30 min under microwave irradiation. The formed precipitate was collected by filtration, washing with *n*-BuOH and then Et₂O to provide 1.25 g of crude **32**, which was used without further purification.

To the crude carboxylic acid from above (**32**, 365 mg, 1.03 mmol) dissolved in DMF (10 mL) were added morpholine (0.110 mL, 1.26 mmol), DIPEA (0.215 mL, 1.24 mmol), and HBTU (469 mg, 1.24 mmol), and the reaction mixture was stirred at room temperature for 1 h. The mixture was diluted with water and extracted with EtOAc (3 × 20 mL), and the combined organic layers were dried (Na₂SO₄), filtered, and concentrated. The residue was purified by preparative HPLC to afford the title compound (246 mg, 56% yield, two steps). ¹H NMR (400 MHz, DMSO-*d*₆) δ 8.38 (s, 1H), 8.30 (s, 1H), 8.16 (d, *J* = 8.2 Hz, 1H), 7.08 (d, *J* = 1.4 Hz, 1H), 7.02 (d, *J* = 8.3 Hz, 1H), 3.98 (s, 3H), 3.89 (s, 3H), 3.61 (br s, 4H), 3.52 (br s, 4H). LCMS, *m/z* = 423 [M + H]⁺.

(2-Chloro-5-methoxy-4-(4-(methylamino)-5-(trifluoromethyl)pyrimidin-2-ylamino)phenyl)(morpholino)methanone (8, Method b). To a solution of 2-chloro-*N*-methyl-5-(trifluoromethyl)pyrimidin-4-amine (**60**, 0.10 g, 0.47 mmol) and (4-amino-2-chloro-5-methoxyphenyl)(morpholino)methanone (**55**, 0.11 g, 0.40 mmol) in *n*-BuOH (2.0 mL) was added TFA (0.051 mL, 0.66 mmol). The mixture was stirred at 75 °C for 2 h. The reaction mixture

was then concentrated. The residue was purified by preparative HPLC to afford 66 mg (37% yield, two steps) of the title compound as a white solid. ¹H NMR (400 MHz, DMSO-*d*₆) δ 8.51 (s, 1H), 8.24 (s, 1H), 8.12 (s, 1H), 7.32 (d, *J* = 4.0 Hz, 1H), 7.06 (s, 1H), 3.89 (s, 3H), 3.49–3.71 (m, 6H), 3.15–3.24 (m, 2H), 2.94 (d, *J* = 4.3 Hz, 3H). LCMS, *m/z* = 446 [M + H]⁺.

(2,5-Dimethoxy-4-(4-(methylamino)-5-(trifluoromethyl)pyrimidin-2-ylamino)phenyl)(piperidin-1-yl)methanone (9, Method e). To a solution of (4-amino-2,5-dimethoxyphenyl)(morpholino)methanone (**59**, 200 mg, 0.750 mmol) in *n*-BuOH (2 mL) were added 2-chloro-*N*-methyl-5-(trifluoromethyl)pyrimidin-4-amine (**60**, 159 mg, 0.750 mmol) and two drops of TFA. The mixture was stirred at 100 °C under microwave irradiation for 1 h. After the mixture was cooled and concentrated, the residue was purified by preparative HPLC to afford the title compound (80 mg, 24% yield, three steps). ¹H NMR (500 MHz, CDCl₃) δ 8.34 (s, 1H), 8.18 (s, 1H), 6.86 (s, 1H), 5.34 (s, 1H), 3.89 (s, 3H), 3.84 (s, 3H), 3.77–3.84 (m, 4H), 3.60–3.66 (m, 2H), 3.28–3.39 (m, 2H), 3.15 (d, *J* = 4.5 Hz, 3H). LCMS, *m/z* = 442 [M + H]⁺.

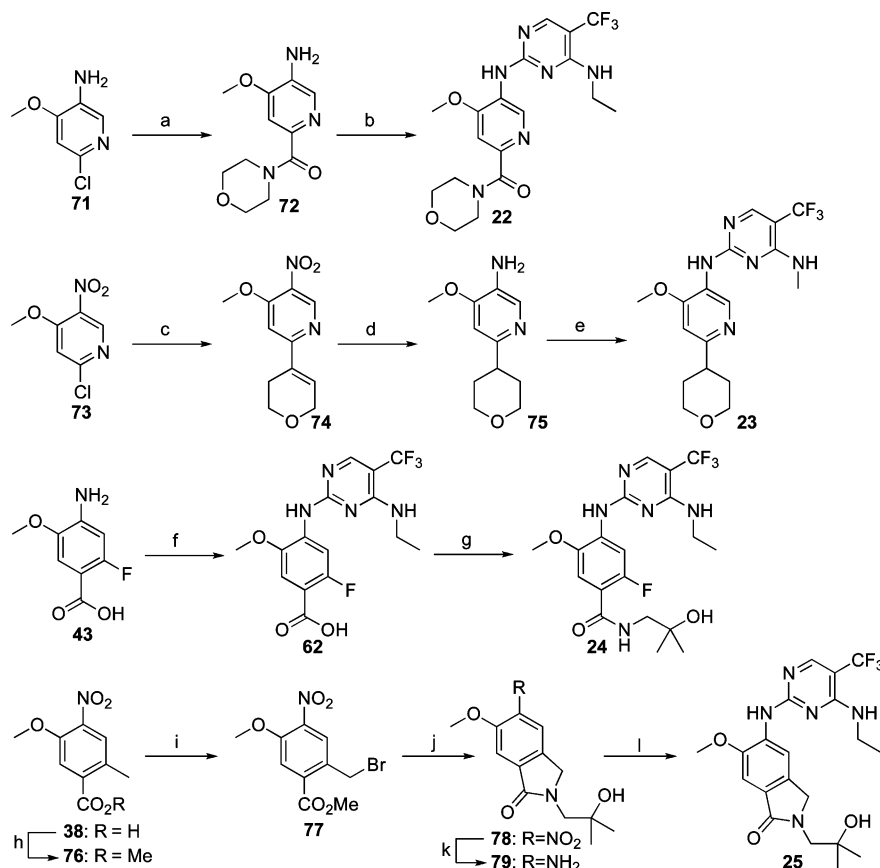
(5-Chloro-2-methoxy-4-(4-(methylamino)-5-(trifluoromethyl)pyrimidin-2-ylamino)phenyl)(morpholino)methanone (10, Method b). The title compound was prepared in a manner analogous to that for **8** (22% yield, two steps). ¹H NMR (400 MHz, DMSO-*d*₆) δ 8.59 (s, 1H), 8.20 (s, 1H), 7.88 (s, 1H), 7.32 (s, 1H), 7.25 (s, 1H), 3.81 (s, 3H), 3.60 (s, 4H), 3.53 (t, *J* = 4.3 Hz, 2H), 3.17 (s, 2H), 2.90 (d, *J* = 4.3 Hz, 3H). LCMS, *m/z* = 446 [M + H]⁺.

(5-Chloro-4-(4-(ethylamino)-5-(trifluoromethyl)pyrimidin-2-ylamino)-2-methoxyphenyl)(morpholino)methanone (11, Method c). A mixture of 2-chloro-*N*-ethyl-5-(trifluoromethyl)pyrimidin-4-amine (**28**; 0.25 g, 1.11 mmol), cesium carbonate (0.72 g, 2.22 mmol), 4-amino-5-chloro-2-methoxyphenyl(morpholino)methanone (**44**; 0.6 g, 2.22 mmol), palladium(II) acetate (5 mg, 0.022 mmol), and Xantphos (19 mg, 0.033 mmol) in degassed dry dioxane (4 mL) was sonicated in an ultrasonic bath for 2 min. The mixture was degassed further with bubbling N₂ for 2 min and heated at 100 °C for 2 h. The mixture was cooled, diluted with EtOAc (25 mL), and washed with water (2 × 20 mL). The combined aqueous washes were extracted with EtOAc (2 × 25 mL). The organic extracts were combined and filtered through a phase separator, and the solvent was removed. Purification of the residue by flash chromatography, 0–100% EtOAc/isohexane, followed by trituration with Et₂O/EtOAc gave the title compound (0.15 g, 30% yield) as a white solid. ¹H NMR (400 MHz, CDCl₃) δ 8.38 (s, 1H), 8.22 (s, 1H), 7.64 (s, 1H), 7.31 (s, 1H), 5.19 (br s, 1H), 3.87 (s, 3H), 3.79–3.77 (m, 4H), 3.65–3.58 (m, 4H), 3.32 (br d, *J* = 14.8 Hz, 2H), 1.30 (t, *J* = 7.6 Hz, 3H); LCMS, *m/z* = 460 [M + H]⁺.

(5-Chloro-4-(4-(ethylamino)-5-(trifluoromethyl)pyrimidin-2-ylamino)-2-methoxyphenyl)(D8-morpholino)methanone (12). The title compound was prepared in a manner analogous to that for **18** (26% yield, two steps). ¹H NMR (400 MHz, CDCl₃) δ 8.38 (s, 1H), 8.22 (s, 1H), 7.64 (br s, 1H), 7.31 (s, 1H), 5.19 (br s, 1H), 3.87 (s, 3H), 3.65–3.58 (m, 2H), 1.30 (t, *J* = 7.2 Hz, 3H). LCMS, *m/z* = 468 [M + H]⁺.

(5-Chloro-2-methyl-4-(4-(methylamino)-5-(trifluoromethyl)pyrimidin-2-ylamino)phenyl)(morpholino)methanone (13, Method d). A mixture of (4-amino-5-chloro-2-methylphenyl)(morpholino)methanone (**56**, 79 mg, 0.31 mmol), 2-chloro-*N*-methyl-5-(trifluoromethyl)pyrimidin-4-amine (**60**, 66 mg, 0.31 mmol), and PTSA (59 mg, 0.31 mmol) in dioxane (4 mL) was heated to 100 °C for 4 h. Saturated sodium bicarbonate solution (10 mL) and CH₂Cl₂ (10 mL) were added, and the organic phase was passed through a hydrophobic frit. The solvent was removed in vacuo and the residue was purified by preparative HPLC to give the title compound (71 mg, 53% yield) as an off-white solid. ¹H NMR (400 MHz, CDCl₃) δ 8.55 (s, 1H), 8.21 (d, *J* = 1.1 Hz, 1H), 7.57 (s, 1H), 7.22 (s, 1H), 5.30 (br s, 1H), 3.79 (br d, *J* = 13.9 Hz, 4H), 3.60 (br s, 2H), 3.32 (br s, 2H), 3.11 (d, *J* = 4.7 Hz, 3H), 2.32 (s, 3H). LCMS, *m/z* = 430 [M + H]⁺.

5-Methoxy-2-methyl-4-(4-(methylamino)-5-(trifluoromethyl)pyrimidin-2-ylamino)phenyl(morpholino)methanone (14 Method d). The title compound was prepared in a

Scheme 6. Synthesis of Pyridine Analogues and Morpholinoamide Derivatives^a

^aReagents and conditions: (a) Mo(CO)₆, Pd(PPh₃)₄, 4-DMAP, DIPEA, morpholine, dioxane, microwave, 50%; (b) **28**, BrettPhos, BrettPhos precatalyst, NaO-*t*-Bu, *t*-BuOH, Δ, 35%; (c) 2-(3,6-dihydro-2*H*-pyran-4-yl)-4,4,5,5-tetramethyl-1,3,2-dioxaborolane, Na₂CO₃, KOAc, Pd(amphos)-Cl₂, CH₃CN, degassed H₂O, microwave, 79%; (d) Pd/C, EtOH, H₂; (e) **60**, BrettPhos, BrettPhos precatalyst, NaO-*t*-Bu, *t*-BuOH, Δ, 52%, two steps; (f) **28**, PTSA, dioxane, Δ; (g) 1-amino-2-methylpropan-2-ol, HATU, DIPEA, CH₂Cl₂, 95%, two steps; (h) SOCl₂, MeOH, Δ, 82%; (i) NBS, CH₃CN, AIBN, Δ, 31%; (j) 1-amino-2-methylpropan-2-ol, Et₃N, MeOH, Δ; (k) Fe dust, EtOH, NH₄Cl, H₂O, Δ, 77%, two steps; (l) PTSA, dioxane, Δ, 33%.

manner analogous to that for **13** (42% yield). ¹H NMR (400 MHz, CDCl₃) δ 8.47 (s, 1H), 8.18 (s, 1H), 7.74 (s, 1H), 6.71 (s, 1H), 5.25 (br s, 1H), 3.88 (s, 3H), 3.80 (br d, *J* = 18.0 Hz, 4H), 3.59 (br s, 2H), 3.31 (br s, 2H), 3.12 (d, *J* = 4.7 Hz, 3H), 2.28 (s, 3H). LCMS, *m/z* = 426 [M + H]⁺.

(5-Fluoro-2-methoxy-4-(4-(methylamino)-5-(trifluoromethyl)pyrimidin-2-ylamino)phenyl)(morpholino)methanone (15, Method d). The title compound was prepared in a manner analogous to that for **13** (20% yield). ¹H NMR (400 MHz, CDCl₃) δ 8.35 (d, *J* = 6.7 Hz, 1H), 8.22 (s, 1H), 7.39 (br s, 1H), 7.07 (d, *J* = 10.6 Hz, 1H), 5.30 (t, *J* = 4.7 Hz, 1H), 3.86 (s, 3H), 3.85–3.73 (m, 4H), 3.63 (br d, *J* = 11.9 Hz, 2H), 3.32 (br d, *J* = 20.3 Hz, 2H), 3.12 (d, *J* = 4.7 Hz, 3H). LCMS, *m/z* = 430 [M + H]⁺.

(2-Fluoro-3-methoxy-4-(4-(methylamino)-5-(trifluoromethyl)pyrimidin-2-ylamino)phenyl)(morpholino)methanone (16, Method g). To a solution of (4-amino-2-fluoro-3-methoxyphenyl)(morpholino)methanone (**58**, 600 mg, 2.36 mmol) in *n*-BuOH (8 mL) was added 2-chloro-*N*-methyl-5-(trifluoromethyl)pyrimidin-4-amine (**60**, 498 mg, 2.36 mmol). The reaction mixture was stirred at 100 °C under microwave irradiation for 1 h. After the mixture was cooled and concentrated, the residue was purified by flash chromatography, 10–33% EtOAc/petroleum ether, to afford a white solid, which was triturated with 10% EtOAc/petroleum ether to afford the title compound as a white solid (700 mg, 69% yield, three steps). ¹H NMR (500 MHz, DMSO-*d*₆) δ 8.52 (s, 1H), 8.21 (s, 1H), 8.11 (d, *J* = 8.5 Hz, 1H), 7.28 (d, *J* = 4.5 Hz, 1H), 7.10–7.07 (m, 1H), 3.90 (d, *J* = 1.5 Hz, 3H), 3.64 (s, 4H), 3.55 (s, 2H), 3.29 (s, 2H), 2.91 (d, *J* = 4.0 Hz, 3H). LCMS, *m/z* = 430 [M + H]⁺.

(2-Fluoro-5-methoxy-4-(4-(methylamino)-5-(trifluoromethyl)pyrimidin-2-ylamino)phenyl)(morpholino)methanone (17, Method e). The title compound was prepared in a manner analogous to that for **9** (40% yield). ¹H NMR (400 MHz, DMSO-*d*₆) δ 8.33 (d, *J* = 12.0 Hz, 1H), 8.25 (s, 1H), 8.11 (s, 1H), 7.35 (q, *J* = 4.3 Hz, 1H), 7.03 (d, *J* = 6.2 Hz, 1H), 3.89 (s, 3H), 3.64–3.55 (m, 6H), 3.32–3.31 (m, 2H), 2.94 (d, *J* = 4.3 Hz, 3H). LCMS, *m/z* = 430 [M + H]⁺.

(4-(4-(ethylamino)-5-(trifluoromethyl)pyrimidin-2-ylamino)-2-fluoro-5-methoxyphenyl)(morpholino)methanone (18). A mixture of 2-chloro-*N*-ethyl-5-(trifluoromethyl)pyrimidin-4-amine (**28**, 70 g, 310 mmol), 4-amino-2-fluoro-5-methoxybenzoic acid (**43**, 49 g, 265 mmol), and PTSA (30 g, 169 mmol) in 1,4-dioxane (400 mL) was stirred at 100 °C for 2 h (the reaction mixture remained as a suspension despite heating). The reaction mixture was then cooled to room temperature. The insoluble solids were collected by filtration, washed with 1,4-dioxane (100 mL) and Et₂O (50 mL), and air-dried for 12 h to give crude 4-(4-(ethylamino)-5-(trifluoromethyl)pyrimidin-2-ylamino)-2-fluoro-5-methoxybenzoic acid **62**. The material (108 g) was used in the next step without further purification.

To a cooled (0 °C) mixture of crude 4-(4-(ethylamino)-5-(trifluoromethyl)pyrimidin-2-ylamino)-2-fluoro-5-methoxybenzoic acid (**62**, 108 g, 289 mmol) in CH₂Cl₂ (500 mL) were added HBTU (125 g, 330 mmol), morpholine (50 mL, 572 mmol), and DIPEA (150 mL, 863 mmol). The reaction mixture was stirred at 0 °C for 15 min before warming to room temperature. The reaction mixture was stirred at room temperature for an additional 45 min. The mixture was then diluted with saturated sodium bicarbonate solution, and the aqueous

layer was extracted with CH_2Cl_2 (2×100 mL). The combined extracts were washed with saturated sodium bicarbonate solution, dried over Na_2SO_4 , filtered, and concentrated.

The crude product was first purified by SFC to give approximately 95 g of desired product. The material was then redissolved in 350 mL of refluxing *i*-PrOH. The solution was allowed to cool slowly (overnight) to room temperature with moderate stirring. The resulting suspension was cooled in an ice bath for 20 min. The solid (83.5 g) was collected by filtration. The isolated solid was redissolved in 400 mL of refluxing *i*-PrOH and allowed to cool to room temperature overnight with stirring. Again, the resulting suspension was cooled in an ice bath for 20 min. The white precipitate was collected by filtration to give a white crystalline solid. The solid was air-dried for 5 h and placed under vacuum for 3 h to give the desired product (74.5 g, 64% yield, two steps). $^1\text{H NMR}$ (400 MHz, CDCl_3) δ 8.44 (d, $J = 12$ Hz, 1H), 8.20 (s, 1H), 7.84 (s, 1H), 6.91 (d, $J = 5.9$ Hz, 1H), 5.21 (br s, 1H), 3.74–3.85 (m, 4H), 3.69–3.71 (m, 2H), 3.58–3.68 (m, 2H), 3.44 (br s, 2H), 1.33 (t, $J = 7.2$ Hz, 3H). LCMS, $m/z = 444$ $[\text{M} + \text{H}]^+$.

(4-(4-(Cyclopropylamino)-5-(trifluoromethyl)pyrimidin-2-ylamino)-2-fluoro-5-methoxyphenyl)(morpholino)methanone (19). The title compound was prepared in a manner analogous to that for **18** (16% yield, two steps). $^1\text{H NMR}$ (400 MHz, CDCl_3) δ 8.77 (d, $J = 12.6$ Hz, 1H), 8.20 (s, 1H), 7.94 (s, 1H), 6.91 (d, $J = 6.0$ Hz, 1H), 5.48 (s, 1H), 3.92 (s, 3H), 3.84–3.76 (m, 4H), 3.68 (t, $J = 4.5$ Hz, 2H), 3.44 (br s, 2H), 2.94–2.87 (m, 1H), 1.03–0.96 (m, 2H), 0.70–0.65 (m, 2H). LCMS, $m/z = 456$ $[\text{M} + \text{H}]^+$.

N^2 -(2-Chloro-4-(1-methyl-1H-tetrazol-5-yl)phenyl)- N^4 -methyl-5-(trifluoromethyl)pyrimidine-2,4-diamine (20). A mixture of N^2 -(2-chloro-4-(2H-tetrazol-5-yl)phenyl)- N^4 -methyl-5-(trifluoromethyl)pyrimidine-2,4-diamine (**66**, 80 mg, 0.22 mmol), K_2CO_3 (45 mg, 0.32 mmol), and methyl iodide (15 μL , 0.24 mmol) in acetone (2 mL) was heated at 40 °C for 1 h. The mixture was cooled and filtered. The filtrate was concentrated under reduced pressure. Purification of the residue by flash chromatography, 0–100% EtOAc/isohexane, gave the title compound (10 mg, 12% yield). $^1\text{H NMR}$ (400 MHz, CDCl_3) δ 8.90 (d, $J = 8.7$ Hz, 1H), 8.24 (s, 1H), 7.86 (d, $J = 2.1$ Hz, 1H), 7.79 (s, 1H), 7.68 (dd, $J = 8.8, 2.1$ Hz, 1H), 5.33 (s, 1H), 4.22 (s, 3H), 3.13 (d, $J = 4.7$ Hz, 3H). LCMS, $m/z = 385$ $[\text{M} + \text{H}]^+$. The isomeric *N*-Me product N^2 -(2-chloro-4-(2-methyl-2H-tetrazol-5-yl)phenyl)- N^4 -methyl-5-(trifluoromethyl)pyrimidine-2,4-diamine (58 mg, 70% yield) was also isolated from the reaction mixture. $^1\text{H NMR}$ (400 MHz, CDCl_3) δ 8.76 (d, $J = 8.7$ Hz, 1H), 8.23–8.19 (m, 2H), 8.05 (dd, $J = 8.7, 2.0$ Hz, 1H), 7.72 (s, 1H), 5.29 (s, 1H), 4.40 (s, 3H), 3.12 (d, $J = 4.7$ Hz, 3H). LCMS, $m/z = 385$ $[\text{M} + \text{H}]^+$.

N^2 -(5-Fluoro-2-methoxy-4-(methylsulfonyl)phenyl)- N^4 -methyl-5-(trifluoromethyl)pyrimidine-2,4-diamine (21). To 5-fluoro-2-methoxy-4-(methylsulfonyl)aniline (**70**, 115.5 mg, 0.53 mmol) and 2-chloro-*N*-methyl-5-(trifluoromethyl)pyrimidin-4-amine (**60**, 117 mg, 0.55 mmol) dissolved in 2-methoxyethanol (5.0 mL, 63 mmol) was added TFA (0.04 mL, 0.53 mmol), and the reaction mixture was heated to 100 °C for 60 h. The mixture was diluted with water and saturated sodium bicarbonate solution, extracted with EtOAc (10 mL), and concentrated under reduced pressure. The residue was purified by flash chromatography, 0–50% EtOAc/heptane, followed by preparative HPLC to afford the title compound (38.9 mg, 19% yield). $^1\text{H NMR}$ (400 MHz, $\text{DMSO}-d_6$) δ 8.58 (d, $J = 13.1$ Hz, 1H), 8.3 (s, 1H), 8.30 (s, 1H), 7.50–7.40 (m, 1H), 7.30 (d, $J = 6.4$ Hz, 1H), 3.96 (s, 3H), 3.29 (s, 3H), 2.96 (d, $J = 4.2$ Hz, 3H). LCMS, $m/z = 395$ $[\text{M} + \text{H}]^+$.

5-(4-(Ethylamino)-5-(trifluoromethyl)pyrimidin-2-ylamino)-4-methoxy-pyridin-2-yl(morpholino)methanone (22). To a vial were added 2-chloro-*N*-ethyl-5-(trifluoromethyl)pyrimidin-4-amine (**28**, 41.8 mg, 0.185 mmol), (5-amino-4-methoxy-pyridin-2-yl)(morpholino)methanone (**72**, 41.9 mg, 0.177 mmol), BrettPhos (9.7 mg, 0.018 mmol), BrettPhos palladium(II) phenethylamine chloride (14.1 mg, 0.018 mmol), and NaO-*t*-Bu (21.0 mg, 0.212 mmol). The vial was purged with N_2 , and *t*-BuOH (2.0 mL) was added. N_2 was bubbled through the reaction mixture for 3 min. Then the vial was capped and heated to 100 °C in an oil bath for 12 h. The reaction mixture was cooled to room temperature, diluted with

CH_2Cl_2 , and filtered through Celite, eluting with CH_2Cl_2 , and the filtrate was concentrated. The residue was adsorbed onto silica and purified by flash chromatography, 0–10% MeOH/ CH_2Cl_2 . The product-containing fractions were combined, concentrated and the residue was further purified by preparative HPLC to give the title compound (26.5 mg, 35% yield) as a white solid. $^1\text{H NMR}$ (400 MHz, $\text{DMSO}-d_6$) δ 8.99 (s, 1H), 8.37 (s, 1H), 8.17 (s, 1H), 7.31 (s, 1H), 7.15 (t, $J = 5.5$ Hz, 1H), 3.93 (s, 3H), 3.70–3.49 (m, 8H), 3.45–3.35 (m, 2H), 1.10 (t, $J = 7.1$ Hz, 3H). LCMS, $m/z = 427$ $[\text{M} + \text{H}]^+$.

N^2 -(4-Methoxy-6-(tetrahydro-2H-pyran-4-yl)pyridin-3-yl)- N^4 -methyl-5-(trifluoromethyl)pyrimidine-2,4-diamine (23). To a round-bottom flask was added 2-(3,6-dihydro-2H-pyran-4-yl)-4-methoxy-5-nitropyridine (**74**, 197 mg, 0.8286 mmol). The flask was purged with N_2 , and EtOH (10 mL) followed by Pd/C (20 wt %, 88 mg, 0.08 mmol) was added. H_2 was bubbled through the solution for 5 min, and the reaction mixture was then stirred overnight at room temperature under an atmosphere of H_2 . The reaction mixture was filtered through Celite, eluting with CH_2Cl_2 , and the filtrate was concentrated to give crude 4-methoxy-6-(tetrahydro-2H-pyran-4-yl)pyridin-3-amine (**75**, 170 mg) that was used without further purification.

To a vial were added 2-chloro-*N*-methyl-5-(trifluoromethyl)pyrimidin-4-amine (**60**, 93 mg, 0.44 mmol), crude 4-methoxy-6-(tetrahydro-2H-pyran-4-yl)pyridin-3-amine (**75**, 87 mg, 0.42 mmol), BrettPhos (23 mg, 0.042 mmol), BrettPhos palladium(II) phenethylamine chloride (33 mg, 0.042 mmol), and NaO-*t*-Bu (50 mg, 0.50 mmol). The vial was purged with N_2 , and *t*-BuOH (3.0 mL) was added. N_2 was bubbled through the reaction mixture for 3 min, and the mixture was then heated to 110 °C in an oil bath for 3 h. The reaction mixture was cooled to room temperature, diluted with CH_2Cl_2 , filtered through Celite, eluting with CH_2Cl_2 , and the filtrate was concentrated. The residue was adsorbed onto silica and purified by flash chromatography, 0–100% EtOAc/heptane. The product-containing fractions were combined, concentrated and the residue was further purified by preparative HPLC to give the title compound (83 mg, 52% yield, two steps) as a white solid. $^1\text{H NMR}$ (400 MHz, $\text{DMSO}-d_6$) δ 8.77 (s, 1H), 8.26 (s, 1H), 8.10 (s, 1H), 7.11–7.04 (m, 1H), 6.98 (s, 1H), 3.99–3.92 (m, 3H), 3.89–3.86 (m, 4H), 3.48–3.39 (m, 3H), 2.93–2.84 (m, 5H), 1.82–1.73 (m, 5H). LCMS, $m/z = 384$ $[\text{M} + \text{H}]^+$.

4-(4-(Ethylamino)-5-(trifluoromethyl)pyrimidin-2-ylamino)-2-fluoro-*N*-(2-hydroxy-2-methylpropyl)-5-methoxybenzamide (24). The title compound was prepared in a manner analogous to that for **18** (95% yield, two steps). $^1\text{H NMR}$ (400 MHz, CDCl_3) δ 8.51 (d, $J = 15.6$ Hz, 1H), 8.21 (s, 1H), 7.93 (s, 1H), 7.58 (d, $J = 7.2$ Hz, 1H), 7.26–7.15 (m, 1H), 5.23 (br s, 1H), 3.96 (s, 3H), 3.65–3.61 (m, 2H), 3.52–3.50 (m, 2H), 1.34 (t, $J = 7.2$ Hz, 3H), 1.21 (s, 6H). LCMS, $m/z = 446$ $[\text{M} + \text{H}]^+$.

5-(4-(Ethylamino)-5-(trifluoromethyl)pyrimidin-2-ylamino)-2-(2-hydroxy-2-methylpropyl)-6-methoxyisoindolin-1-one (25). The synthesis of **25** was carried out using the same procedure as that for **13**, method d (38 mg, 33%). $^1\text{H NMR}$ (400 MHz, CDCl_3) δ 8.69 (s, 1H), 8.21 (s, 1H), 7.95 (s, 1H), 7.33 (s, 1H), 5.18 (br s, 1H), 4.53 (s, 2H), 3.98 (s, 3H), 3.63–3.56 (m, 4H), 3.39 (s, 1H), 1.34–1.32 (m, 3H), 1.30 (s, 6H). LCMS, $m/z = 439$ $[\text{M} + \text{H}]^+$.

2-Chloro-*N*-ethyl-5-(trifluoromethyl)pyrimidin-4-amine (28). Into a 3000 mL four-necked round-bottom flask purged and maintained with an inert atmosphere of N_2 was placed copper(I) iodide (224 g, 1.17 mmol) and potassium fluoride (68 g, 1.17 mmol). The mixture was heated to 150 °C under reduced pressure for 2 h. After the mixture was cooled to room temperature, a solution of trimethyl(trifluoromethyl)silane (167 g, 1.17 mmol) in DMF (500 mL) and NMP (500 mL) was added by syringe. The mixture was stirred for 30 min, followed by the addition of a solution of 2-chloro-5-iodo-4-methoxy-pyrimidine (**26**, 278 g, 980.6 mmol) in DMF (500 mL) and NMP (500 mL) by syringe. The resulting solution was stirred at 35 °C for 48 h and quenched by the addition of 10 L of water. The solids were filtered out. The filtrate was extracted with EtOAc (3×5000 mL). The combined organic layers were washed with brine (3×2000 mL), dried over Na_2SO_4 , and concentrated. The residue was

purified by flash chromatography, 0–5% EtOAc/petroleum ether, to afford the title compound (153 g, 69% yield) as a white solid. ^1H NMR (300 MHz, CDCl_3) δ 8.25 (s, 1H), 5.40 (s, 1H), 3.66–3.57 (m, 2H), 1.32–1.27 (t, $J = 7.2$ Hz, 3H). LCMS, $m/z = 226$ $[\text{M} + \text{H}]^+$.

2-Chloro-*N*-cyclopropyl-5-(trifluoromethyl)pyrimidin-4-amine (29). To 2,4-dichloro-5-(trifluoromethyl)pyrimidine (27, 1.25 g, 5.8 mmol) in MeOH (4 mL) at 0 °C was added cyclopropylamine (0.69 mL, 10 mmol). The mixture was allowed to stir at room temperature for 4 h, and then CH_2Cl_2 (20 mL) and water (20 mL) were added. The mixture was passed through a hydrophobic frit, and the solvent was removed. Purification of the residue by flash chromatography, 0–100% CH_2Cl_2 /isohexane, gave the title compound (472 mg, 34% yield) as an off-white solid. ^1H NMR (400 MHz, CDCl_3) δ 8.27 (d, $J = 1.1$ Hz, 1H), 5.56 (br s, 1H), 3.03–2.93 (m, 1H), 0.99–0.89 (m, 2H), 0.65–0.60 (m, 2H). LCMS, $m/z = 238$ $[\text{M} + \text{H}]^+$.

5-Chloro-2-methyl-4-nitrobenzonitrile (34). To 5-chloro-2-methyl-4-nitroaniline (33, 5 g, 26.8 mmol) in a mixture of acetone (17.5 mL) and water (19 mL) at 0 °C was added concentrated HCl (5.6 mL). A solution of sodium nitrite (2.25 g, 32.6 mmol) in water (7.5 mL) was added dropwise, and the mixture was allowed to stir at 0 °C for 30 min. The mixture was then added dropwise to a mixture of copper cyanide (3.75 g, 42 mmol) and sodium cyanide (5.5 g, 112 mmol) in water (25 mL) and EtOAc (12.5 mL). The mixture was allowed to stir at room temperature for 1 h, and then water (50 mL) was added. The mixture was extracted with EtOAc (3 \times 100 mL), and the combined organic fractions were washed with 2 M $\text{NaOH}_{(\text{aq})}$ (50 mL) and brine (50 mL). The organic fraction was passed through a hydrophobic frit, and the solvent was removed in vacuo. The residue was suspended in a 1:1 mixture of diethyl ether/isohexane. The solid formed was removed by filtration and washed with isohexane and dried. Further fractions were isolated from the filtrate and combined with the initial solid fraction to give the title compound (3.22 g, 61% yield) as an off-white solid. ^1H NMR (400 MHz, CDCl_3) δ 7.80 (s, 1H), 7.80 (s, 1H), 2.63 (s, 3H). LCMS, $m/z = 197$ $[\text{M} + \text{H}]^+$.

5-Methoxy-2-methyl-4-nitrobenzonitrile (36). The title compound was prepared in a manner analogous to that for 34 (90% yield). ^1H NMR (400 MHz, CDCl_3) δ 7.72 (s, 1H), 7.31 (s, 1H), 3.98 (s, 3H), 2.55 (s, 3H). LCMS, $m/z = 192$ $[\text{M} + \text{H}]^+$.

5-Chloro-2-methyl-4-nitrobenzoic Acid (37). A mixture of 5-chloro-2-methyl-4-nitrobenzonitrile (34, 1 g, 5 mmol) in AcOH (10 mL), water (10 mL), and concentrated H_2SO_4 (10 mL) was heated to 120 °C for 5 h. Water (100 mL) was added and the solid was removed by filtration and dried to give the title compound (905 mg, 84% yield) as an off-white solid. ^1H NMR (400 MHz, CDCl_3) δ 8.22 (s, 1H), 7.76 (s, 1H), 2.70 (s, 3H). LCMS, $m/z = 214$ $[\text{M} + \text{H}]^+$.

5-Methoxy-2-methyl-4-nitrobenzoic Acid (38). The title compound was prepared in a manner analogous to that for 37 (58% yield). ^1H NMR (400 MHz, CDCl_3) δ 7.75 (s, 1H), 7.70 (s, 1H), 3.99 (s, 3H), 2.62 (s, 3H). LCMS, $m/z = 210$ $[\text{M} + \text{H}]^+$.

4-Amino-5-fluoro-2-methoxybenzonitrile (40). To a stirred solution of MeOH (26 mL) in THF (15 mL) under N_2 was added *t*-BuOK (1.5 g, 13.0 mmol) in small portions over 10 min. The resulting solution was stirred at room temperature for 5 min, and then 4-amino-2,5-difluorobenzonitrile (39, 1.0 g, 6.5 mmol) was added. The mixture was then warmed to 70 °C and stirred for 3.5 h. The mixture was cooled and diluted with EtOAc (25 mL), washed with water and brine, dried over MgSO_4 , and concentrated to dryness under reduced pressure. The residue was triturated with diethyl ether/isohexane to afford the title compound (0.86 g, 80% yield). ^1H NMR (400 MHz, CDCl_3) δ 7.15 (d, $J = 10.4$ Hz, 1H), 6.26 (d, $J = 7.2$ Hz, 1H), 4.25 (br s, 2H), 3.84 (s, 3H). LCMS, $m/z = 167$ $[\text{M} + \text{H}]^+$.

4-Amino-5-fluoro-2-methoxybenzoic Acid (41). A solution of 4-amino-5-fluoro-2-methoxybenzonitrile (40, 250 mg, 1.51 mmol) and KOH in a mixture of EtOH (5 mL) and water (5 mL) was heated at reflux for 30 h. The mixture was cooled and treated with 30% aqueous H_2O_2 (0.25 mL). The mixture was stirred for 10 min and then heated to reflux for 18 h. After return to room temperature, water (3 mL) was added and 6 N HCl solution was added until pH 4 was obtained. The mixture was filtered and the collected solid was washed with a small

amount of water and dried at 50 °C under vacuum to afford the title compound (190 mg, 68% yield). ^1H NMR (400 MHz, $\text{DMSO}-d_6$) δ 11.8 (br s, 1H), 7.40 (d, $J = 12.0$ Hz, 1H), 6.44 (d, $J = 8.0$ Hz, 1H), 6.00 (br s, 2H), 3.75 (s, 3H). LCMS, $m/z = 186$ $[\text{M} + \text{H}]^+$.

(4-Amino-5-chloro-2-methoxyphenyl)(morpholino)methanone (44). The title compound was prepared in a manner analogous to that for 46 (carried forward as crude yellow paste). LCMS, $m/z = 271$ $[\text{M} + \text{H}]^+$.

(4-Amino-5-fluoro-2-methoxyphenyl)(morpholino)methanone (45). The title compound was prepared in a manner analogous to that for 46 (72% yield). ^1H NMR (400 MHz, CDCl_3) δ 8.02 (s, 2H), 6.95 (d, $J = 10.5$ Hz, 1H), 6.30 (d, $J = 7.1$ Hz, 1H), 3.76 (s, 3H), 3.72–3.64 (m, 4H), 3.58 (t, $J = 4.9$ Hz, 2H), 3.40 (t, $J = 4.9$ Hz, 2H). LCMS, $m/z = 255$ $[\text{M} + \text{H}]^+$.

(4-Amino-2-fluoro-5-methoxyphenyl)(morpholino)methanone (46). A mixture of 4-amino-2-fluoro-5-methoxybenzoic acid (43, 4.2 g, 22.7 mmol), HATU (10.4 g, 27.2 mmol), and morpholine (5 mL, 56.8 mmol) in CH_2Cl_2 was stirred in a cold water bath, and DIPEA (10 mL, 56.8 mmol) was added. After 10 min the mixture was allowed to warm to room temperature and stirred for 1 h. The mixture was diluted with CH_2Cl_2 (100 mL) and washed with saturated sodium bicarbonate solution (3 \times 75 mL) and water (100 mL). The separated organic phase was passed through a hydrophobic frit, and the solvent was concentrated. The crude product was triturated with CH_2Cl_2 / Et_2O and the filtered solid dried under vacuum to give the title compound (4.10 g, 71% yield) as an off-white solid. ^1H NMR (400 MHz, CDCl_3) δ 6.80 (d, $J = 6.0$ Hz, 1H), 6.36 (d, $J = 10.7$ Hz, 1H), 4.12 (s, 2H), 3.84 (s, 3H), 3.83–3.61 (m, 6H), 3.42 (s, 2H). LCMS, $m/z = 255$ $[\text{M} + \text{H}]^+$.

(4-Amino-2-chloro-5-methoxyphenyl)(morpholino)methanone (50). The title compound was prepared in a manner analogous to that for 46 (63% yield). ^1H NMR (400 MHz, $\text{DMSO}-d_6$) δ 8.14 (s, 1H), 7.47 (s, 1H), 3.95 (s, 3H), 3.51–3.72 (m, 6H), 3.15–3.19 (m, 2H). LCMS, $m/z = 301$ $[\text{M} + \text{H}]^+$.

(5-Chloro-2-methyl-4-nitrophenyl)(morpholino)methanone (51). The title compound was prepared in a manner analogous to that for 46 (95% yield). ^1H NMR (400 MHz, CDCl_3) δ 7.76 (s, 1H), 7.36 (s, 1H), 3.83–3.76 (m, 4H), 3.66–3.58 (m, 2H), 3.28–3.20 (m, 2H), 2.37 (s, 3H). LCMS, $m/z = 285$ $[\text{M} + \text{H}]^+$.

(5-Methoxy-2-methyl-4-nitrophenyl)(morpholino)methanone (52). The title compound was prepared in a manner analogous to that for 46 (59% yield). ^1H NMR (400 MHz, CDCl_3) δ 7.72 (s, 1H), 6.90 (s, 1H), 3.94 (s, 3H), 3.85–3.76 (m, 4H), 3.61 (dd, $J = 5.7, 4.0$ Hz, 2H), 3.23 (dd, $J = 5.7, 4.0$ Hz, 2H), 2.30 (s, 3H). LCMS, $m/z = 281$ $[\text{M} + \text{H}]^+$.

(2-Fluoro-3-methoxy-4-nitrophenyl)(morpholino)methanone (53). The title compound was prepared in a manner analogous to that for 46 (carried forward as crude). LCMS, $m/z = 285$ $[\text{M} + \text{H}]^+$.

(2,5-Dimethoxy-4-nitrophenyl)(morpholino)methanone (54). The title compound was prepared in a manner analogous to that for 46 (carried forward as crude). LCMS, $m/z = 297$ $[\text{M} + \text{H}]^+$.

(4-Amino-2-chloro-5-methoxyphenyl)(morpholino)methanone (55). To a solution of (2-chloro-5-methoxy-4-nitrophenyl)(morpholino)methanone (50, 825 mg, 2.74 mmol) in EtOH (10 mL) were added iron dust (0.90 g, 16 mmol), NH_4Cl (0.90 g, 17 mmol), and water (0.5 mL). The suspension was stirred at 90 °C under a N_2 atmosphere for 1 h. The reaction mixture was allowed to cool to room temperature and filtered through a pad of Celite. The filtrate was concentrated. The resulting solid residue was resuspended in EtOAc, sonicated for 1 min, and filtered. The filtrate was concentrated to give the crude title compound (743 mg), which was used without further purification. LCMS, $m/z = 271$ $[\text{M} + \text{H}]^+$.

(4-Amino-5-chloro-2-methylphenyl)(morpholino)methanone (56). To (5-chloro-2-methyl-4-nitrophenyl)(morpholino)methanone (51, 244 mg, 0.86 mmol) in EtOH (6 mL) and water (0.6 mL) was added $\text{SnCl}_4 \cdot 2\text{H}_2\text{O}$ (776 mg, 3.44 mmol). The mixture was heated to 65 °C for 5 h, and then 2 M aqueous sodium hydroxide solution (10 mL) and CH_2Cl_2 (10 mL) were added. The organic phase was passed through a hydrophobic frit and the solvent was removed in vacuo to give the title compound (203

mg, 93% yield) as an off-white solid. ^1H NMR (400 MHz, CDCl_3) δ 7.07 (s, 1H), 6.60 (s, 1H), 4.10 (br s, 2H), 3.84–3.53 (br m, 6H), 3.36–3.24 (br m, 2H), 2.21 (s, 3H). LCMS, $m/z = 255$ $[\text{M} + \text{H}]^+$.

(4-Amino-5-methoxy-2-methylphenyl)(morpholino)methanone (57). The title compound was prepared in a manner analogous to that for 56 (92% yield). ^1H NMR (400 MHz, CDCl_3) δ 6.60 (s, 1H), 6.52 (s, 1H), 3.87–3.52 (br m, 6H), 3.84 (br s, 2H), 3.82 (s, 3H), 3.36–3.23 (br m, 2H), 2.17 (s, 3H). LCMS, $m/z = 251$ $[\text{M} + \text{H}]^+$.

(4-Amino-2-fluoro-3-methoxyphenyl)(morpholino)methanone (58). To a mixture of (2-fluoro-3-methoxy-4-nitrophenyl)(morpholino)methanone (53, 1.2 g, 4.2 mmol) in MeOH (50 mL) was added Pd/C (10 wt %, 100 mg). The reaction mixture was stirred under H_2 (1 atm) at room temperature for 1 h. The insoluble material was filtered off and the filtrate was concentrated under reduced pressure to afford the crude title compound as a white solid, which was used without further purification. LCMS, $m/z = 255$ $[\text{M} + \text{H}]^+$.

(4-Amino-2,5-dimethoxyphenyl)(morpholino)methanone (59). The title compound was prepared in a manner analogous to that for 58 (carried forward as crude). LCMS, $m/z = 267$ $[\text{M} + \text{H}]^+$.

3-Chloro-4-(4-(methylamino)-5-(trifluoromethyl)pyrimidin-2-ylamino)benzotrile (65). A mixture of 2-chloro-*N*-methyl-5-(trifluoromethyl)pyrimidin-4-amine (60, 211 mg, 1 mmol), 4-amino-3-chlorobenzotrile (64, 305 mg, 2 mmol), cesium carbonate (0.65 g, 2 mmol), Xantphos (17 mg, 0.03 mmol), and $\text{Pd}_2(\text{dba})_3$ (5 mg, 0.02 mmol) in dioxane (3 mL) was sonicated in an ultrasonic bath for 1 min. The mixture was then degassed under a stream of N_2 for 5 min. The tube was sealed, and the mixture was heated at 100 °C for 18 h. The reaction mixture was cooled and diluted with EtOAc (15 mL). The organic layer was washed with water (2 \times 20 mL), and the combined aqueous extracts were further washed with EtOAc (2 \times 15 mL). The combined organics were passed through a phase separation cartridge, and the solvent was removed under reduced pressure. Purification of the residue by flash chromatography, 0–100% EtOAc/isohexane, gave the title compound as a white solid (140 mg, 45% yield). ^1H NMR (400 MHz, CDCl_3) δ 8.85 (d, $J = 8.8$ Hz, 1H); 8.23 (d, $J = 1.1$ Hz, 1H), 7.80 (s, 1H), 7.68 (d, $J = 1.9$ Hz, 1H), 7.58–7.53 (m, 1H); 5.32 (br s, 1H), 3.11 (d, $J = 4.7$ Hz, 3H). LCMS, $m/z = 328$ $[\text{M} + \text{H}]^+$.

N^2 -(2-Chloro-4-(2H-tetrazol-5-yl)phenyl)- N^4 -methyl-5-(trifluoromethyl)pyrimidine-2,4-diamine (66). To a solution of 3-chloro-4-(4-(methylamino)-5-(trifluoromethyl)pyrimidin-2-ylamino)benzotrile (65, 135 mg, 6.41 mmol) in DMF (2 mL) were added NaN_3 (80 mg, 1.24 mmol) and NH_4Cl (66 mg, 1.24 mmol). The mixture was heated at 125 °C for 18 h. The mixture was cooled, filtered and the solid washed with EtOAc. The filtrate was concentrated under reduced pressure, and the crude residue was diluted with water (5 mL) and Et_2O (5 mL). A precipitate formed which was filtered and washed with further portions of water and Et_2O . The solid was coevaporated with CH_2Cl_2 and MeOH and then dried in a vacuum oven to yield the title compound (130 mg, 85% yield). ^1H NMR (400 MHz, $\text{DMSO}-d_6$) δ 8.94 (s, 1H), 8.26–8.19 (m, 2H), 8.14 (d, $J = 2.0$ Hz, 1H), 8.03–7.96 (m, 1H), 7.30–7.22 (m, 1H), 2.89 (t, $J = 4.4$ Hz, 3H). LCMS, $m/z = 371$ $[\text{M} + \text{H}]^+$.

(2-Fluoro-5-methoxy-4-nitrophenyl)(methyl)sulfane (68). To 1,2-difluoro-4-methoxy-5-nitrobenzene (67, 0.72 g, 3.8 mmol) in EtOH (100 mL) was added sodium thiomethoxide (0.30 g, 4.1 mmol) in water (0.96 mL, 53 mmol), and the reaction mixture was heated to reflux for 3 h. The solvent was removed under reduced pressure and the residue was purified by flash chromatography, 0–40% EtOAc/heptane, to afford the title compound (0.75 g, 91% yield). ^1H NMR (400 MHz, CDCl_3) δ 7.68 (d, $J = 9.3$ Hz, 1H), 6.83 (d, $J = 6.1$ Hz, 1H), 3.98 (s, 3H), 2.55 (s, 3H). LCMS, $m/z =$ not detected.

1-Fluoro-4-methoxy-2-(methylsulfonyl)-5-nitrobenzene (69). (2-Fluoro-5-methoxy-4-nitrophenyl)(methyl)sulfane (68, 0.75 g, 3.5 mmol) was dissolved in CH_2Cl_2 (30 mL), and *m*-CPBA (77% pure) (1.0 g, 4.5 mmol) was added portionwise. The mixture was stirred for 16 h at room temperature. Additional *m*-CPBA (77% pure) (1.5 g, 6.92 mmol) was added and the mixture stirred for another 24 h

at room temperature. The solvent was removed under reduced pressure and the residue was purified by flash chromatography, 0–50% EtOAc/heptane, to afford the title compound (0.41 g, 48% yield). ^1H NMR (400 MHz, CDCl_3) δ 7.72 (d, $J = 8.3$ Hz, 1H), 7.68 (d, $J = 5.2$ Hz, 1H), 4.03 (s, 3H), 3.28 (s, 3H). LCMS, $m/z =$ not detected.

5-Fluoro-2-methoxy-4-(methylsulfonyl)aniline (70). To 1-fluoro-4-methoxy-2-(methylsulfonyl)-5-nitrobenzene (69, 0.41 g, 1.6 mmol) in EtOH (80 mL) was added Pd/C (10 wt %, 18 mg, 0.16 mmol), and the reaction mixture was stirred under H_2 (1 atm) for 12 h. The reaction mixture was filtered through Celite, and the solvents were removed under reduced pressure. The residue was purified by flash chromatography, 0–70% EtOAc/heptane, to afford the title compound (0.36 g, 99% yield). ^1H NMR (400 MHz, CDCl_3) δ 7.19 (d, $J = 6.2$ Hz, 1H), 7.46 (d, $J = 11.0$ Hz, 1H), 4.44 (s, 3H), 3.88 (s, 3H), 3.16 (s, 3H). LCMS, $m/z = 220$ $[\text{M} + \text{H}]^+$.

(5-Amino-4-methoxypyridin-2-yl)(morpholino)methanone (72). To a microwave vial were added 6-chloro-4-methoxypyridin-3-amine (71, 100 mg, 0.63 mmol), molybdenum hexacarbonyl (183 mg, 0.69 mmol), $\text{Pd}(\text{PPh}_3)_4$ (36.5 mg, 0.03 mmol), and 4-DMAP (46.7 mg, 0.38 mmol). 1,4-Dioxane (10 mL) was then added followed by DIPEA (0.22 mL, 1.26 mmol) and morpholine (0.66 mL, 7.57 mmol). N_2 was then bubbled through reaction mixture for 3 min. Then the vial was capped and heated to 150 °C in a microwave for 40 min. The reaction mixture was then filtered through Celite, eluting with CH_2Cl_2 , and the filtrate was concentrated. The crude residue was adsorbed onto silica and purified by flash chromatography, 0–10% MeOH/ CH_2Cl_2 , to give the title compound (75 mg, 50% yield) as a beige foam. ^1H NMR (300 MHz, CDCl_3) δ 8.25 (s, 1H), 5.40 (s, 1H), 3.66–3.57 (m, 2H), 1.32–1.27 (t, $J = 7.2$ Hz, 3H). LCMS, $m/z = 238$ $[\text{M} + \text{H}]^+$.

2-(3,6-Dihydro-2H-pyran-4-yl)-4-methoxy-5-nitropyridine (74). To a microwave vial were added 2-chloro-4-methoxy-5-nitropyridine (73, 200 mg, 1.06 mmol), 2-(3,6-dihydro-2H-pyran-4-yl)-4,4,5,5-tetramethyl-1,3,2-dioxaborolane (312 mg, 1.48 mmol), Na_2CO_3 (158 mg, 1.48 mmol), bis(*di-tert*-butyl(4-dimethylaminophenyl)phosphine)dichloropalladium(II) (75 mg, 0.11 mmol), and KOAc (147 mg, 1.48 mmol). CH_3CN (10 mL) and degassed water (2 mL) were added, and N_2 was bubbled through the solution for 3 min. The vial was capped and submitted to microwave heating at 140 °C for 40 min. The reaction mixture was diluted with CH_2Cl_2 , filtered through Celite, eluting with CH_2Cl_2 , and the filtrate was concentrated. The crude residue was adsorbed onto silica and purified by flash chromatography, 0–100% EtOAc/heptane, to give the title compound (197 mg, 79% yield). ^1H NMR (300 MHz, CDCl_3) δ 8.25 (s, 1H), 5.40 (s, 1H), 3.66–3.57 (m, 2H), 1.32–1.27 (t, $J = 7.2$ Hz, 3H). LCMS, $m/z = 237$ $[\text{M} + \text{H}]^+$.

Methyl 5-Methoxy-2-methyl-4-nitrobenzoate (76). To 5-methoxy-2-methyl-4-nitrobenzoic acid (38, 1.27 g, 6 mmol) in MeOH (15 mL) was added SOCl_2 (0.44 mL, 6 mmol) dropwise. The mixture was heated to reflux for 3 h and then allowed to cool. The solvent was removed, and the residue was partitioned between CH_2Cl_2 (20 mL) and saturated sodium bicarbonate solution (20 mL). The organic phase was passed through a hydrophobic frit, and the solvent was removed. Purification of the residue by flash chromatography, 0–100% EtOAc/isohexane, gave the title compound (1.11 g, 82% yield) as an off-white solid. ^1H NMR (400 MHz, CDCl_3) δ 7.68 (s, 1H), 7.60 (s, 1H), 3.98 (s, 3H), 3.95 (s, 3H), 2.55 (s, 3H). LCMS, $m/z = 226$ $[\text{M} + \text{H}]^+$.

Methyl 2-(Bromomethyl)-5-methoxy-4-nitrobenzoate (77). A mixture of methyl 5-methoxy-2-methyl-4-nitrobenzoate (76, 1.11 g, 5 mmol) and NBS (1.07 g, 6 mmol) in MeCN (20 mL) was degassed, and then AIBN (18 mg, 0.11 mmol) was added. The mixture was heated to 70 °C for 18 h. CH_2Cl_2 (50 mL) and water (50 mL) were added, and the organic phase was passed through a hydrophobic frit. The solvent was removed, and purification of the residue by flash chromatography, 0–100% EtOAc/isohexane, gave the title compound (477 mg, 31% yield) as an off-white solid. ^1H NMR (400 MHz, CDCl_3) δ 7.92 (s, 1H), 7.66 (s, 1H), 4.88 (s, 2H), 4.02 (s, 3H), 4.00 (s, 3H). LCMS, $m/z = 304$ $[\text{M} + \text{H}]^+$.

2-(2-Hydroxy-2-methylpropyl)-6-methoxy-5-nitroisindolin-1-one (78). To methyl 2-(bromomethyl)-5-methoxy-4-nitrobenzoate (77, 220 mg, 0.72 mmol) in MeOH (6 mL) were added Et₃N (0.12 mL, 0.86 mmol) and 1-amino-2-methylpropan-2-ol (77 mg, 0.86 mmol). The mixture was heated to 70 °C for 5 h, and then EtOAc (30 mL) and 1 M HCl_(aq) (30 mL) were added. The layers were separated, and the aqueous layer was extracted with EtOAc (2 × 30 mL). The combined organic fractions were passed through a hydrophobic frit, and the solvent was removed. The residue was used directly in the next reaction without any purification. LCMS, *m/z* = 281 [M + H]⁺.

5-Amino-2-(2-hydroxy-2-methylpropyl)-6-methoxyisindolin-1-one (79). To crude 2-(2-hydroxy-2-methylpropyl)-6-methoxy-5-nitroisindolin-1-one (78, 0.72 mmol) in a mixture of EtOH (15 mL) and water (1.5 mL) were added iron powder (134 mg, 2.4 mmol) and NH₄Cl (160 mg, 3 mmol). The resulting mixture was heated at 80 °C for 18 h, then cooled to room temperature, filtered through a pad of Celite, and rinsed through with MeOH. The filtrate was evaporated, and the residue was dissolved in CH₂Cl₂ (100 mL) and washed with water (3 × 50 mL). The organic phase was dried over MgSO₄, filtered, and concentrated under reduced pressure to give the title compound (138 mg, 77% yield, two steps). ¹H NMR (400 MHz, CDCl₃) δ 7.21 (s, 1H), 6.68 (s, 1H), 4.40 (br s, 2H), 4.21 (s, 2H), 3.90 (s, 3H), 3.74 (s, 1H), 3.55 (s, 2H), 1.27 (s, 6H). LCMS, *m/z* = 251 [M + H]⁺.

Molecular Modeling. Homology models of LRRK2 were constructed using the modeling program MOE, version 2009.10 (Chemical Computing Group, Montreal),⁶² and AMBER99⁶³ force field. The human LRRK2 sequence was retrieved from Swiss-Prot⁶⁴ and aligned to template structure sequences using ClustalW⁶⁵ followed by manual fine-tuning of residues adjacent to loop regions, insertions, and deletions. The models were further refined with bound ligand using the MacroModel utility implemented in Maestro and OPLS2005 force field (Schrödinger, Inc., New York, NY).⁶⁶ Inhibitor docking studies were carried out using docking program Glide SP with one hydrogen bond constrained to the carbonyl oxygen of hinge residue Ala1950. The docking poses were evaluated based on a combination of criteria including the Glide docking score (cutoff of -6), favorable intermolecular interactions with the hinge and other parts of the ATP-binding pocket, and low strain energy of the bound ligand (*E*_{strain} < 2 kcal/mol).

■ ASSOCIATED CONTENT

Supporting Information

Spleen PK/PD graphs for 14, 18, and 19 and additional experimental procedures. This material is available free of charge via the Internet at <http://pubs.acs.org>.

■ AUTHOR INFORMATION

Corresponding Author

*Phone: 650-225-4934. Fax: 650-742-4943. E-mail: estrada.anthony@gene.com.

Present Address

▽ Novartis Institutes for Biomedical Research (NIBR), 4560 Horton Street, Emeryville, CA 94608-2916.

Notes

The authors declare no competing financial interest.

■ ACKNOWLEDGMENTS

We thank the Analytical, Bioanalytical, NMR, Pharmacokinetic, Biopharmacology, and Safety Assessment colleagues for their contributions. We thank Vivienne Allen, Linda Bao, Leo Berezhkovskiy, Po-Chang Chiang, Kang-Jye Chou, Jason Halladay, Quynh Ho, Claire Holt, Heather Kennedy, Emile Plise, Veronica Rivera, Kimberley Smith, Hilda Solano, and Hervé Van de Poël for their individual contributions. We also thank Dr. Zhenyu Yue and his group at the Mount Sinai School

of Medicine for kindly providing the G2019S BAC transgenic mice.

■ ABBREVIATIONS USED

LRRK2, leucine-rich repeat kinase 2; CNS, central nervous system; PD, Parkinson's disease; JAK2, Janus kinase 2; MMP, matched molecular pair; MPO, multiparameter optimization; LLE, lipophilic ligand efficiency; LELP, ligand-efficiency-dependent lipophilicity; P-gp, P-glycoprotein; MDCK-MDR1, Madin–Darby canine kidney cells-multidrug resistance protein 1; ER, efflux ratio; CSF, cerebrospinal fluid; PPB, plasma protein binding; BPB, brain protein binding; AUC, area under the curve; BAC, bacterial artificial chromosome; FVB, Friend virus B-type; PEG, polyethylene glycol; NMP, *N*-methyl-2-pyrrolidone; MCT, methylcellulose/Tween

■ REFERENCES

- (1) Lees, A. J.; Hardy, J.; Revesz, T. Parkinson's disease. *Lancet* **2009**, *373*, 2055–2066. Erratum in *Lancet* **2009**, *374*, 684.
- (2) Zimprich, A.; Biskup, S.; Leitner, P.; Lichtner, P.; Farrer, M.; Lincoln, S.; Kachergus, J.; Hulihan, M.; Uitti, R. J.; Calne, D. B.; Stoessl, A. J.; Pfeiffer, R. F.; Patenge, N.; Carbajal, I. C.; Vieregge, P.; Asmus, F.; Muller-Myhsok, B.; Dickson, D. W.; Meitinger, T.; Strom, T. M.; Wszolek, Z. K.; Gasser, T. Mutations in LRRK2 cause autosomal-dominant parkinsonism with pleomorphic pathology. *Neuron* **2004**, *44*, 601–607.
- (3) Paisan-Ruiz, C.; Jain, S.; Evans, E. W.; Gilks, W. P.; Simon, J.; van der Brug, M.; Lopez de Munain, A.; Aparicio, S.; Gil, A. M.; Khan, N.; Johnson, J.; Martinez, J. R.; Nicholl, D.; Carrera, I. M.; Pena, A. S.; de Silva, R.; Lees, A.; Marti-Masso, J. F.; Perez-Tur, J.; Wood, N. W.; Singleton, A. B. Cloning of the gene containing mutations that cause PARK8-linked Parkinson's disease. *Neuron* **2004**, *44*, 595–600.
- (4) Mata, I. F.; Wedemeyer, W. J.; Farrer, M. J.; Taylor, J. P.; Gallo, K. A. LRRK2 in Parkinson's disease: protein domains and functional insights. *Trends Neurosci.* **2006**, *29*, 286–293.
- (5) Greggio, E.; Cookson, M. R. Leucine-rich repeat kinase 2 mutations and Parkinson's disease: three questions. *ASN Neuro* **2009**, *1*, e00002.
- (6) Gandhi, P. N.; Chen, S. G.; Wilson-Delfosse, A. L. Leucine-rich repeat kinase 2 (LRRK2): a key player in the pathogenesis of Parkinson's disease. *J. Neurosci. Res.* **2009**, *87*, 1283–1295.
- (7) Dachselt, J. C.; Farrer, M. J. LRRK2 and Parkinson disease. *Arch. Neurol.* **2010**, *67*, 542–547.
- (8) Satake, W.; Nakabayashi, Y.; Mizuta, I.; Hirota, Y.; Ito, C.; Kubo, M.; Kawaguchi, T.; Tsunoda, T.; Watanabe, M.; Takeda, A.; Tomiyama, H.; Nakashima, K.; Hasegawa, K.; Obata, F.; Yoshikawa, T.; Kawakami, H.; Sakoda, S.; Yamamoto, M.; Hattori, N.; Murata, M.; Nakamura, Y.; Toda, T. Genome-wide association study identifies common variants at four loci as genetic risk factors for Parkinson's disease. *Nat. Genet.* **2009**, *41*, 1303–1307.
- (9) Simón-Sánchez, J.; Schulte, C.; Bras, J. M.; Sharma, M.; Gibbs, J. R.; Berg, D.; Paisan-Ruiz, C.; Lichtner, P.; Scholz, S. W.; Hernandez, D. G.; Krüger, R.; Federoff, M.; Klein, C.; Goate, A.; Perlmutter, J.; Bonin, M.; Nalls, M. A.; Illig, T.; Gieger, C.; Houlden, H.; Steffens, M.; Okun, M. S.; Racette, B. A.; Cookson, M. R.; Foote, K. D.; Fernandez, H. H.; Traynor, B. J.; Schreiber, S.; Arepalli, S.; Zonozzi, R.; Gwinn, K.; van der Brug, M.; Lopez, G.; Chanock, S. J.; Schatzkin, A.; Park, Y.; Hollenbeck, A.; Gao, J.; Huang, X.; Wood, N. W.; Lorenz, D.; Deuschl, G.; Chen, H.; Riess, O.; Hardy, J. A.; Singleton, A. B.; Gasser, T. Genome-wide association study reveals genetic risk underlying Parkinson's disease. *Nat. Genet.* **2009**, *41*, 1308–1312.
- (10) West, A. B.; Moore, D. J.; Biskup, S.; Bugayenko, A.; Smith, W. W.; Ross, C. A.; Dawson, V. L.; Dawson, T. M. Parkinson's disease-associated mutations in leucine-rich repeat kinase 2 augment kinase activity. *Proc. Natl. Acad. Sci. U.S.A.* **2005**, *102*, 16842–16847.
- (11) Greggio, E.; Jain, S.; Kingsbury, A.; Bandopadhyay, R.; Lewis, P.; Kaganovich, A.; van der Brug, M. P.; Beilina, A.; Blackinton, J.;

Thomas, K. J.; Ahmad, R.; Miller, D. W.; Kesavapany, S.; Singleton, A.; Lees, A.; Harvey, R. J.; Harvey, K.; Cookson, M. R. Kinase activity is required for the toxic effects of mutant LRRK2/dardarin. *Neurobiol. Dis.* **2006**, *23*, 329–341.

(12) Cookson, M. R. The role of leucine-rich repeat kinase 2 (LRRK2) in Parkinson's disease. *Nat. Rev. Neurosci.* **2010**, *11*, 791–797.

(13) Rudenko, I. N.; Chia, R.; Cookson, M. R. Is inhibition of kinase activity the only therapeutic strategy for LRRK2-associated Parkinson's disease? *BMC Med.* **2012**, *10*, 20–27.

(14) Liu, Z.; Hamamichi, S.; Lee, B. D.; Yang, D.; Ray, A.; Caldwell, G. A.; Caldwell, K. A.; Dawson, T. M.; Smith, W. W.; Dawson, V. L. Inhibitors of LRRK2 kinase attenuate neurodegeneration and Parkinson-like phenotypes in *Caenorhabditis elegans* and *Drosophila* Parkinson's disease models. *Hum. Mol. Genet.* **2011**, *20*, 3933–3942.

(15) Lee, B. D.; Shin, J.-H.; VanKampen, J.; Petrucelli, L.; West, A. B.; Ko, H. S.; Lee, Y.-I.; Maguire-Zeiss, K. A.; Bowers, W. J.; Federoff, H. J.; Dawson, V. L.; Dawson, T. M. Inhibitors of leucine-rich repeat kinase-2 protect against models of Parkinson's disease. *Nat. Med.* **2010**, *16*, 998–1000.

(16) For a recent review on LRRK2 small molecule kinase inhibitors, see the following: Kramer, T.; Lo Monte, F.; Göring, S.; Amombo, G. M. O.; Schmidt, B. Small molecule kinase inhibitors for LRRK2 and their application to Parkinson's disease models. *ACS Chem. Neurosci.* **2012**, *3*, 151–160.

(17) Lee, B. D.; Dawson, V. L.; Dawson, T. M. Leucine-rich repeat kinase 2 (LRRK2) as a potential therapeutic target in Parkinson's disease. *Trends Pharmacol. Sci.* **2012**, *33*, 365–373.

(18) Deng, X.; Dzakmo, N.; Prescott, A.; Davies, P.; Liu, Q.; Yang, Q.; Lee, J.-D.; Patricelli, M. P.; Nomanbhoy, T. K.; Alessi, D. R.; Gray, N. S. Characterization of a selective inhibitor of the Parkinson's disease kinase LRRK2. *Nat. Chem. Biol.* **2011**, *7*, 203–205.

(19) Ramsden, N.; Perrin, J.; Ren, Z.; Lee, B. D.; Zinn, N.; Dawson, V. L.; Tam, D.; Bova, M.; Lang, M.; Drewes, G.; Bantscheff, M.; Bard, F.; Dawson, T. M.; Hopf, C. Chemoproteomics-based design of potent LRRK2-selective lead compounds that attenuate Parkinson's disease-related toxicity in human neurons. *ACS Chem. Biol.* **2011**, *6*, 1021–1028.

(20) Nichols, P. L.; Eatheron, A. J.; Bamborough, P.; Jandu, K. S.; Philps, O. J.; Andreotti, D. Novel Compounds. WO 2011/038572 A1, 2011.

(21) Lewis, P. A.; Manzoni, C. LRRK2 and human disease: a complicated question or a question of complexes? *Sci. Signaling* **2012**, *5*, pe2.

(22) Drolet, R. E.; Sanders, J. M.; Kern, J. T. Leucine-rich repeat kinase 2 (LRRK2) cellular biology: a review of recent advances in identifying physiological substrates and cellular functions. *J. Neurogenet.* **2011**, *25*, 140–151.

(23) Zhang, J.; Deng, X.; Choi, H. G.; Alessi, D. R.; Gray, N. S. Characterization of TAE684 as a potent LRRK2 kinase inhibitor. *Bioorg. Med. Chem. Lett.* **2012**, *22*, 1864–1869.

(24) Sheng, Z.; Zhang, S.; Bustos, Z.; Kleinheinz, T.; Le Pichon, C. E.; Dominguez, S. L.; Solanoy, H. O.; Drummond, J.; Zhang, X.; Ding, X.; Cai, F.; Song, Q.; Li, X.; Yue, Z.; van der Brug, M. P.; Burdick, D. J.; Gunzner-Toste, J.; Chen, H.; Liu, X.; Estrada, A. A.; Sweeney, Z. K.; Scarce-Levie, K.; Moffat, J. G.; Kirkpatrick, D. S.; Zhu, H. Ser1292 autophosphorylation is a biomarker of LRRK2 kinase activity and mediates cellular effects of PD mutations. *Sci. Transl. Med.* **2012**, in press.

(25) Chen, H.; Chan, B. K.; Drummond, J.; Estrada, A. A.; Gunzner-Toste, J.; Liu, X.; Liu, Y.; Moffat, J. G.; Shore, D.; Sweeney, Z. K.; Tran, T.; Wang, S.; Zhao, G.; Zhu, H.; Burdick, D. J. Discovery of selective LRRK2 inhibitors guided by computational analysis and molecular modeling. *J. Med. Chem.* **2012**, *55*, 5536–5545.

(26) Li, X.; Patel, J. C.; Wang, J.; Avshalumov, M. V.; Nicholson, C.; Buxbaum, J. D.; Elder, G. A.; Rice, M. E.; Yue, Z. Enhanced striatal dopamine transmission and motor performance with LRRK2 over-expression in mice is eliminated by familial Parkinson's disease mutation G2019S. *J. Neurosci.* **2010**, *30*, 1788–1797.

(27) Hu, X.; Hu, Y.; Vogt, M.; Stumpfe, D.; Bajorath, J. MMP-Cliffs: systematic identification of activity cliffs on the basis of matched molecular pairs. *J. Chem. Inf. Model.* **2012**, *52*, 1138–1145.

(28) Muller, K. The power of MMPA and a teaching lesson in medicinal chemistry. *J. Med. Chem.* **2012**, *55*, 1815–1816.

(29) Stumpfe, D.; Bajorath, J. Exploring activity cliffs in medicinal chemistry. *J. Med. Chem.* **2012**, *55*, 2932–2942.

(30) Griffen, E.; Leach, A. G.; Robb, G. R.; Warner, D. J. Matched molecular pairs as a medicinal chemistry tool. *J. Med. Chem.* **2011**, *54*, 7739–7750.

(31) Hu, Y.; Bajorath, J. Chemical transformations that yield compounds with distinct activity profiles. *ACS Med. Chem. Lett.* **2011**, *2*, 523–527.

(32) Milletti, F.; Hermann, J. C. Targeted kinase selectivity from kinase profiling data. *ACS Med. Chem. Lett.* **2012**, *3*, 383–386.

(33) Galkin, A. V.; Melnick, J. S.; Kim, S.; Hood, T. L.; Li, N.; Li, L.; Xia, G.; Steensma, R.; Chopiuk, G.; Jiang, J.; Wan, Y.; Ding, P.; Liu, Y.; Sun, F.; Schultz, P. G.; Gray, N. S.; Warmuth, M. Identification of NVP-TAE684, a potent, selective, and efficacious inhibitor of NPM-ALK. *Proc. Natl. Acad. Sci. U.S.A.* **2007**, *104*, 270–275; Erratum in *Proc. Natl. Acad. Sci. U.S.A.* **2007**, *104*, 2025.

(34) Anderson, D. R.; Meyers, M. J.; Vernier, W. F.; Mahoney, M. W.; Kurumbail, R. G.; Caspers, N.; Poda, G. I.; Schindler, J. F.; Reitz, D. B.; Mourey, R. J. Pyrrolopyridine inhibitors of mitogen-activated protein kinase activated protein kinase 2 (MK-2). *J. Med. Chem.* **2007**, *50*, 2647–2654.

(35) Baker-Glenn, C.; Burdick, D. J.; Chambers, M.; Chan, B. K.; Chen, H.; Estrada, A.; Gunzner, J. L.; Shore, D.; Sweeney, Z. K.; Wang, S.; Zhao, G. Aminopyrimidine derivatives as LRRK2 modulators and their preparation and use for the treatment of Parkinson's disease. WO2011151360A1, 2011.

(36) Choi, H. G.; Zhang, J.; Deng, X.; Hatcher, J. M.; Patricelli, M. P.; Zhao, Z.; Alessi, D. R.; Gray, N. S. Brain penetrant LRRK2 inhibitor. *ACS Med. Chem. Lett.* **2012**, *3*, 658–662.

(37) Wager, T. T.; Hou, X.; Verhoest, P. R.; Villalobos, A. Moving beyond the rules: the development of a central nervous system multiparameter optimization (CNS MPO) approach to enable alignment of druglike properties. *ACS Chem. Neurosci.* **2010**, *1*, 435–449.

(38) Leeson, P. D.; Springthorpe, B. The influence of drug-like concepts on decision-making in medicinal chemistry. *Nat. Rev. Drug Discovery* **2007**, *6*, 881–890.

(39) Keserü, G. M.; Makara, G. M. The influence of lead discovery strategies on the properties of drug candidates. *Nat. Rev. Drug Discovery* **2009**, *8*, 203–212.

(40) For impact of lipophilic efficiency parameters on compound quality, see the following: Tarcsay, A.; Nyíri, K.; Keserü, G. M. Impact of lipophilic efficiency on compound quality. *J. Med. Chem.* **2012**, *55*, 1252–1260. For impact on CNS drugs and candidates, see the following: Wager, T. T.; Chandrasekaran, R. Y.; Hou, X.; Troutman, M. D.; Verhoest, P. R.; Villalobos, A.; Will, Y. Defining desirable central nervous system drug space through the alignment of molecular properties, in vitro ADME, and safety attributes. *ACS Chem. Neurosci.* **2010**, *1*, 420–434.

(41) Liu, X.; Ding, X.; Deshmukh, G.; Liederer, B. M.; Hop, C. E. C. A. Use of cassette dosing approach to assess brain penetration in drug discovery. *Drug Metab. Dispos.* **2012**, *40*, 963–969.

(42) Hennig, L.; Ayala-Leon, K.; Angulo-Cornejo, J.; Richter, R.; Beyer, L. Fluorine hydrogen short contacts and hydrogen bonds in substituted benzamides. *J. Fluorine Chem.* **2009**, *130*, 453–460.

(43) Fritz, H.; Winkler, T. Weitreichende kopplung zwischen protonen und fluor in 2-fluorbenzamidinen. *Helv. Chim. Acta* **1974**, *57*, 836–839.

(44) Hitchcock, S. A. Structural modifications that alter the P-glycoprotein efflux properties of a compound. *J. Med. Chem.* **2012**, *55*, 4877–4895.

(45) Lovering, F.; Bikker, J.; Humblet, C. Escape from Flatland: increasing saturation as an approach to improving clinical success. *J. Med. Chem.* **2009**, *52*, 6752–6756.

- (46) Ishikawa, M.; Hashimoto, Y. Improvement in aqueous solubility in small molecule drug discovery programs by disruption of molecular planarity and symmetry. *J. Med. Chem.* **2011**, *54*, 1539–1554.
- (47) Liu, X.; Smith, B. J.; Chen, C.; Callegari, E.; Becker, S. L.; Chen, X.; Cianfronga, J.; Doran, A. C.; Doran, S. D.; Gibbs, J. P.; Hosea, N.; Liu, J.; Nelson, F. R.; Szewc, M. A.; Van Deusen, J. Evaluation of cerebrospinal fluid concentration and plasma free concentration as a surrogate measurement for brain free concentration. *Drug Metab. Dispos.* **2006**, *34*, 1443–1447.
- (48) Lin, J. H. CSF as a surrogate for assessing CNS exposure: an industrial perspective. *Curr. Drug Metab.* **2008**, *9*, 46–59.
- (49) Invitrogen Lanthascreen Eu kinase binding assay kit for TTK.
- (50) Kwiatkowski, N.; Jelluma, N.; Filippakopoulos, P.; Sundararajan, M.; Manak, M. S.; Kwon, M.; Choi, H. G.; Sim, T.; Deveraux, Q. L.; Rottmann, S.; Pellman, D.; Shah, J. V.; Kops, G. J. P.; Knapp, S.; Gray, N. S. Small-molecule kinase inhibitors provide insight into Mps1 cell cycle function. *Nat. Chem. Biol.* **2010**, *6*, 359–368.
- (51) Olaharski, A. J.; Gonzaludo, N.; Bitter, H.; Goldstein, D.; Kirchner, S.; Uppal, H.; Kolaja, K. Identification of a kinase profile that predicts chromosome damage induced by small molecule kinase inhibitors. *PLoS Comput. Biol.* **2009**, *5*, e1000446.
- (52) Lan, W.; Cleveland, D. W. A chemical tool box defines mitotic and interphase roles for Mps1 kinase. *J. Cell Biol.* **2010**, *190*, 21–24.
- (53) Wilberg, K. B. The deuterium isotope effect. *Chem. Rev.* **1955**, *55*, 713.
- (54) Hitchcock, S. A.; Pennington, L. D. Structure–brain exposure relationships. *J. Med. Chem.* **2006**, *49*, 7559–7583.
- (55) Fabian, M. A.; Biggs, W. H.; Treiber, D. K.; Atteridge, C. E.; Azimioara, M. D.; Benedetti, M. G.; Carter, T. A.; Ciceri, P.; Edeen, P. T.; Floyd, M.; Ford, J. M.; Galvin, M.; Gerlach, J. L.; Grotzfeld, R. M.; Herrgard, S.; Insko, D. E.; Insko, M. A.; Lai, A. G.; Lélias, J.-M.; Mehta, S. A.; Milanov, Z. V.; Velasco, A. M.; Wodicka, L. M.; Patel, H. K.; Zarrinkar, P. P.; Lockhart, D. J. A small molecule–kinase interaction map for clinical kinase inhibitors. *Nat. Biotechnol.* **2005**, *23*, 329–336.
- (56) Porter, R. H.; Benwell, K. R.; Lamb, H.; Malcolm, C. S.; Allen, N. H.; Revell, D. F.; Adams, D. R.; Sheardown, M. J. Functional characterization of agonists at recombinant human 5-HT_{2A}, 5-HT_{2B} and 5-HT_{2C} receptors in CHO-K1 cells. *Br. J. Pharmacol.* **1999**, *128*, 13–20.
- (57) Zhou, S.-F.; Wang, B.; Yang, L.-P.; Liu, J.-P. Structure, function, regulation and polymorphism and the clinical significance of human cytochrome P450 1A2. *Drug Metab. Rev.* **2010**, *42*, 268–354.
- (58) Zhou, S.-F.; Yang, L.-P.; Zhou, Z.-W.; Liu, Y.-H.; Chan, E. Insights into the substrate specificity, inhibitors, regulation, and polymorphisms and the clinical impact of human cytochrome P450 1A2. *AAPS J.* **2009**, *11*, 481–494.
- (59) Cellular assay is triple mutant LRRK2 (R1441G/Y1699C/G2019S), and BAC transgenic mice are G2019S mutant LRRK2.
- (60) Akabane, T.; Tabata, K.; Kadono, K.; Sakuda, S.; Terashita, S.; Teramura, T. A comparison of pharmacokinetics between humans and monkeys. *Drug Metab. Dispos.* **2010**, *38*, 308–316.
- (61) Roller, S.; Cui, D.; Laspina, C.; Miller-Stein, C.; Rowe, J.; Wong, B.; Prueksaranont, T. Preclinical pharmacokinetics of MK-0974, an orally active calcitonin-gene related peptide (CGRP)-receptor antagonist, mechanism of dose dependency and species differences. *Xenobiotica* **2009**, *39*, 33–45.
- (62) MOE, version 2009.10; Chemical Computing Group Inc.: Montreal, Quebec, Canada.
- (63) Wang, J.; Cieplak, P.; Kollman, P. A. How well does a restrained electrostatic potential (RESP) model perform in calculating conformational energies of organic and biological molecules? *J. Comput. Chem.* **2000**, *21*, 1049.
- (64) Bairoch, A.; Boeckmann, B.; Ferro, S.; Gasteiger, E. Swiss-Prot: juggling between evolution and stability. *Briefings Bioinf.* **2004**, *5*, 39–55.
- (65) Thompson, J. D.; Higgins, D. G.; Gibson, T. J. CLUSTAL W: improving the sensitivity of progressive multiple sequence alignment through sequence weighting, position specific gap penalties and weight matrix choice. *Nucleic Acids Res.* **1994**, *22*, 4673–4680.
- (66) *Maestro Suites*, version 2009; Schrödinger, Inc.: New York, 2009.